ELSEVIER

Journal of Fluids and Structures 26 (2010) 92–120

JOURNAL OF FLUIDS AND STRUCTURES

www.elsevier.com/locate/jfs

Flow-excited resonance of trapped modes of ducted shallow cavities

K. Aly*, S. Ziada

Department of Mechanical Engineering, McMaster University, 1280 Main Street West, Hamilton, Ontario, Canada L8S 4L7

Received 9 March 2009; accepted 3 August 2009

Abstract

The self-excitation mechanism of the acoustic diametral modes of an axisymmetric internal cavity–duct system is studied for a Mach number range up to 0.4. The effect of cavity dimensions on the excitation mechanism is investigated experimentally and numerically. Experiments are conducted on three cavity depths and six cavity lengths for each depth. Numerical simulations of the mode shapes are also performed to determine the effect of cavity dimensions on the particle velocity field of the diametral modes. For all the tested configurations, the diametral modes are strongly excited at relatively low Mach numbers (as low as 0.1). The pulsation amplitude at resonance is found to increase as the cavity becomes shorter or deeper, relative to the main pipe diameter. The test results provide new insights into the excitation mechanism of diametral modes, the effect of the cavity length to depth ratio on the Strouhal numbers of acoustic resonances caused by various shear-layer modes of the cavity, and into the effect of the particle velocity field of the acoustic modes on the mode selectivity mechanism which determines the dominant acoustic mode during resonance.

Keywords: Shallow cavity; Diametral mode; Acoustic resonance

1. Introduction

Flow over cavities has been a source of acoustic noise and mechanical vibration in many engineering applications. The interest in this phenomenon was first driven by problems related to the naval and aeronautical industries (Krishnamurty, 1955; Rossiter, 1962). Later, oscillation problems in combustion chambers and rocket engines (Flandro, 1986) were attributed to flow over cavities. More recently, flow over cavities has been extensively investigated because of its wide range of applications such as piping system (Lafon et al., 2003), control valves (Ziada and Bühlmann, 1989), aero-optical applications (Ahuja and Chambers, 1987), flows over car open windows or sunroofs (Kook et al., 1997), and many others.

Despite the geometrical simplicity, the self-excitation mechanism of cavity oscillations involves several complex fluid mechanics phenomena. The two main components of this mechanism are the inherent instability of the cavity shear layer and a feedback phenomenon. The latter phenomenon depends on the nature of system oscillation. Rockwell and Naudascher (1978) classified these oscillations into three categories, depending on the nature of the feedback phenomenon: (i) fluid-dynamic, (ii) fluid-resonant, and (iii) fluid-elastic oscillations. This paper deals with the

*Corresponding author. Tel.: +1 905 962 7590.
E-mail address: awnykm@mcmaster.ca (K. Aly).

0889-9746/$ - see front matter © 2009 Elsevier Ltd. All rights reserved.
doi:10.1016/j.jfluidstructs.2009.07.008

fluid-resonant mechanism in piping systems, in which the feedback effect is produced by the velocity fluctuations resulting from acoustic resonance. The feedback cycle of events in this mechanism starts when the unstable shear layer is triggered at the cavity leading edge by small vorticity perturbations. These perturbations grow rapidly as they are convected downstream by the mean flow. As these amplified vorticity perturbations reach the cavity downstream corner, part of the energy of the vortical structures is transferred into acoustic energy due to the interaction between the vorticity field and the acoustic field. When the phasing of these events is favourable, the generated acoustic energy amplifies or sustains the acoustic resonance mode of the cavity. The velocity fluctuation associated with the acoustic resonance then triggers the shear layer at the cavity leading edge, which closes the feedback cycle. It is clear from this cycle of events that the nature of the acoustic mode, including its spatial compatibility with the shear layer oscillation mode, has a strong effect on whether this feedback mechanism can be self-sustained or not.

The excitation mechanisms of various acoustic modes of piping systems have been investigated by many authors. This includes the excitation of depth modes in closed side branches and deep cavities, the resonance of longitudinal modes of piping systems containing multiple orifice plates, axisymmetric cavities or corrugations, as well as the excitation of cross (or higher order) acoustic modes in ducts housing a single or multiple bluff bodies. The mechanism of flow-excited acoustic resonance of closed side-branches has been investigated by many researchers including, among others, Bruggeman et al. (1991), Ziada and Bühlmann (1992), Kriesels et al. (1995), Ziada and Shine (1999) and Dequand et al. (2003). In this configuration, the excited acoustic mode is a longitudinal mode of the side branch, and is generally coupled with the main pipe acoustics. Using the discrete vortex model, Nelson et al. (1983) and Bruggeman et al. (1991) proposed a two-dimensional theoretical model for the acoustic source at the side-branch mouth to predict the acoustic and hydrodynamic conditions required for the self-sustained excitation. More recently, Kriesels et al. (1995) and Dequand et al. (2003) developed more elaborate models to predict the resonance range of flow velocity and the amplitude of acoustic pulsations. Although all these models are basically two-dimensional and neglect the three-dimensional effects of the flow, their predictions agree reasonably well with the experimental data. This good agreement is due to the fact that the wavelength of the acoustic mode is substantially longer than the diameter of the side-branch, which ensures uniform acoustic *phase distribution* over the shear layer at the branch mouth.

The flow oscillation between two tandem orifice plates installed inside a circular pipe was found to be capable of strongly exciting the piping system longitudinal modes (Nomoto and Culick, 1982). Hourigan et al. (1990) studied experimentally and numerically the excitation of longitudinal acoustic modes by flow in a duct containing two sets of baffles. They found the phase between the acoustic mode and the vortex travelling past the downstream baffle to be the controlling parameter for having sound power generation from the free shear layer or not. For this configuration, the wavelength of the acoustic mode is larger than both the pipe perimeter and the distance between the two baffles, which allowed two-dimensional modelling of the problem as the acoustic oscillation is in phase over the pipe cross-section. Rockwell and Schachenmann (1982) and Geveci et al. (2003), among many others, investigated the similar problem of coupling between the shear layer of a cylindrical cavity and the longitudinal resonance modes of the associated piping.

Impinging free shear-layer oscillation can also excite duct cross-modes. Stoneman et al. (1988) showed that the cavity free shear-layer-like oscillation in the gap between two tandem plates in a duct can excite strongly the duct cross-modes. Lafon et al. (2003) and Ziada et al. (2003) demonstrated experimentally the excitation of two-dimensional duct cross-modes by the shear layer of a cavity attached to one side-wall of the duct. Also, Lafon et al. (2003) simulated the excitation process numerically. For this type of resonance, the acoustic modes are two-dimensional and the acoustic oscillation is in phase along the whole width, or the spanwise length, of the free shear layer.

The work presented in this paper focuses on the excitation of the trapped acoustic modes, also called the diametral or the cross-modes, of an axisymmetric cavity–duct system. For this type of modes, the wavelength is smaller than the pipe perimeter, and therefore the acoustic phase changes along the azimuthal direction, not the longitudinal direction, which is in contrast with longitudinal pipe modes or the side-branch modes. Therefore, the phase of the free shear-layer oscillation in the azimuthal direction, which corresponds to the spanwise direction in the two-dimensional problem, is expected to be highly modulated by the acoustic field. This modulation makes the problem highly three-dimensional and consequently different from previously studied configurations and acoustic modes.

Hein and Koch (2008) calculated the mode shapes and frequencies of different diametral modes of axisymmetric cavity–duct system at *zero flow velocity*. They showed that these modes consist of transverse waves with frequencies lower than the cut-off frequency of the duct. According to Kinsler et al. (2000), transverse waves in wave guides with frequency lower than the cut-off frequency of the wave guide, such as those simulated by Hein and Koch (2008) for a cavity–duct system, do not propagate down the wave guide (duct), and for the case of the cavity–duct system their amplitude decays exponentially along the duct with the distance from the cavity. Therefore, these are trapped modes which are "locked" to the cavity and experience negligibly small acoustic radiation from the ends of a finite duct. The excitation of such a mode has been reported for various valve configurations, including, for example, gate valves as reported by Smith and Luloff (2000) and Lafon et al. (2003).

Only a few studies investigated the excitation of duct-trapped modes by flow over shallow cavities. Keller and Escudier (1983) performed limited tests on an axisymmetric cavity using a blow-down wind tunnel. They reported resonance of a diametral acoustic mode at a very high transonic flow speed. No details had been given about the flow conditions over which the diametral mode was excited. Davies (1981) reported the excitation of diametral modes; however, the cavity geometry was more like an axisymmetric Helmholtz resonator. Accordingly, there is not much known about the geometrical or hydrodynamic conditions that favour the excitation of diametral modes.

Reviewing the literature indicates that the cavity geometry affects the behaviour of cavity oscillation. Several authors have investigated the effect of cavity length to depth ratio, L/d, on the *fluid-dynamic mechanism* of cavity oscillation. Sarohia (1977) characterized a minimum length for the cavity to exhibit fluid-dynamic oscillations. He based the value of the minimum length on the upcoming boundary layer thickness and the cavity depth. Ahuja and Mendoza (1995) and Tracy and Plentovich (1993) showed that in the case of fluid-dynamic oscillation, the level of the noise generation by flow over cavities decreases with the increase of cavity length and increases with the increase of cavity depth. Similar behaviour was observed by Rockwell et al. (2003) for the excitation of *longitudinal acoustic modes* of a cavity–duct system.

On the other hand, the effect of cavity length, L, and depth, d, on the excitation of the *diametral modes* of internal cavities, to the authors' knowledge, has never been investigated to date. Therefore, one of the objectives of this paper is to determine the effect of changing both the cavity length and depth, relative to the diameter of the duct, D, on the excitation process. In total, 18 different cavities are investigated, including three cavity depths and six cavity lengths for each depth. With the exception of one case, all tested cavities are classified as shallow cavities, with length to depth ratios in the range of $L/d = 1$–12. Numerical simulations are also performed to better understand the effect of the cavity dimensions on the particle velocity distributions of various acoustic modes, and thereby delineate the mechanism of selecting the preferred mode of oscillation.

2. Experimental details

2.1. Cavity set-up

As shown in Fig. 1, the test-section consisted of two 150 mm in inner diameter clear acrylic pipes. Each pipe had a length of $\mathscr{L} = 450$ mm and a wall thickness of 6.25 mm. The criteria of choosing the different dimensions of the pipe will be discussed in the next section. These two pipes were separated by means of a series of acrylic flanges which had a larger inner diameter to form an axisymmetric internal cavity. Two flanges, glued to the pipes, were used to attach the two pipes to the flanges forming the cavity. The details of the flanges forming the cavity are shown in Fig. 2. They were machined on a CNC machine to ensure dimensional accuracy and had wall thickness of 25 mm to provide high rigidity at the area of pressure antinode. Increasing the cavity wall stiffness reduces the acoustic losses due to the vibrations of the cavity wall; also a stiffer wall prevents geometrical deformations during the assembly.

Three sets of flanges with 175, 200 and 250 mm in inner diameter (D+2d) were made to test cavity depths of $d = 12.5$, 25 and 50 mm, respectively. These depths are equivalent to depth to pipe diameter ratios of $d/D = 1/12$, 2/12 and 4/12, respectively. Each set of flanges consisted of 9 pieces; two end discs, five flanges 25 mm in thickness and two flanges 12.5 mm in thickness. With this set-up, the cavity length L could be changed from 25 to 150 mm with a step of 25 mm for the three cavity depths. This arrangement facilitated that the pressure transducers were always positioned at the middle of the cavity length. The tested cavity length to depth ratios varied from 0.5 to 12 as listed in Table 1. Threaded rods were used to fasten all the parts together and O-rings were used to seal all the interfaces between the different parts of the test-section, as shown in Fig. 2. This prevents air leakage from/to the test-section and thereby minimizes the acoustic loses due to the fluctuation of the air leakage with the acoustic pressure.

At the inlet side of the test-section (see Fig. 1), a parabolic contraction was used to produce a uniform inlet velocity profile and to minimize both the turbulence level and the pressure drop. The outlet side of the test-section was connected to the suction side of a centrifugal blower by means of axisymmetric diffuser. The flow velocity in the test-section was controlled by varying the blower speed by means of a 50 HP motor and a speed controller.

2.2. Instrumentation

A pitot-tube located directly downstream the bell-mouth contraction was used to measure the dynamic head at the centreline of the test-section. At this section, the flow velocity was found uniform within 0.5%, as was verified with several measurements over the cross-section. The Pitot tube was connected to a Validyne diaphragm type differential

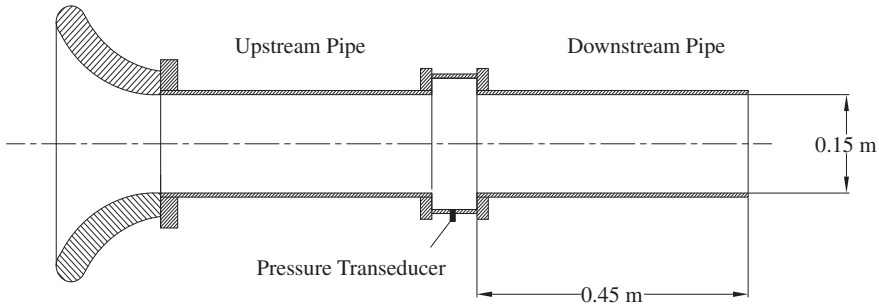

Fig. 1. Schematic drawing of the test-section showing the inlet bell-mouth and the axisymmetric cavity–duct system.

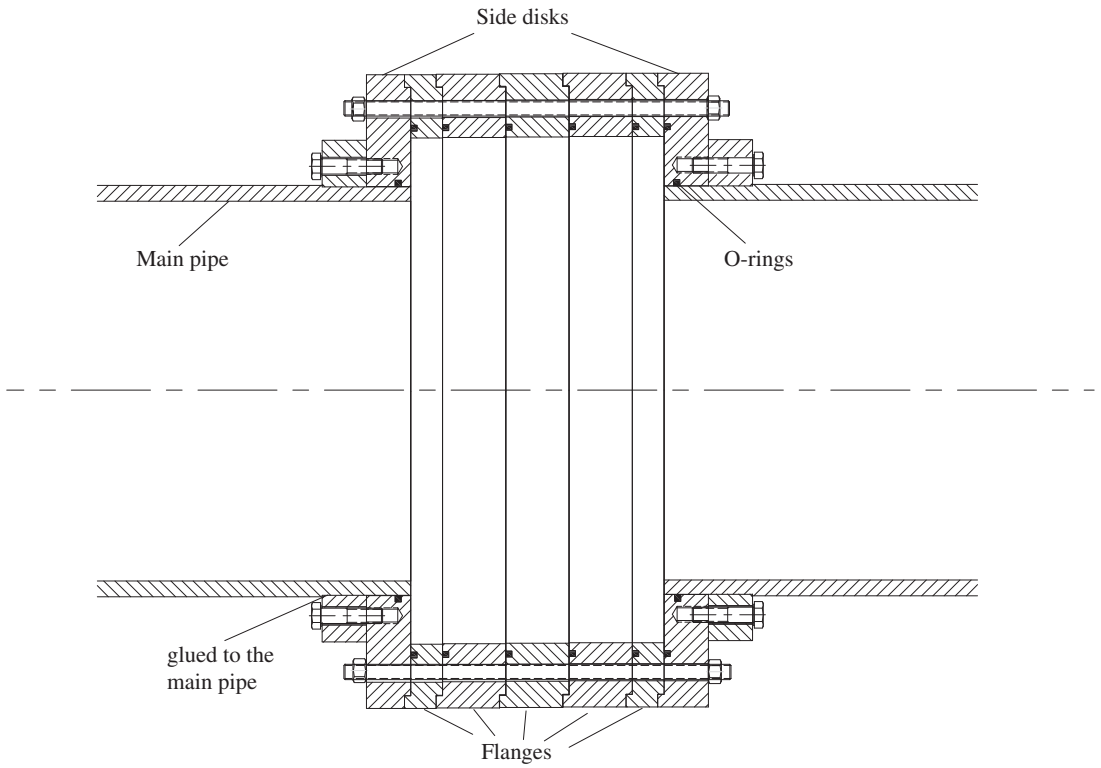

Fig. 2. Schematic drawing of the cavity design. Cavity depth is 25 mm and cavity length is 100 mm.

Table 1
Dimensions of tested cavities.

d (mm)	Ratio d/D	Tested ratios of L/d
12.5	1/12	2, 4, 6, 8, 10, 12
25	2/12	1, 2, 3, 4, 5, 6
50	4/12	0.5, 1, 1.5, 2, 2.5, 3

pressure transducer model no. DP45-14. The electrical bridge of the pressure transducer was adjusted using a pressure pump and an accurately calibrated pressure transducer. This secondary calibration procedure was repeated several times to estimate the uncertainty. The standard deviation in the calibration procedure was found to be 0.5% of the full scale.

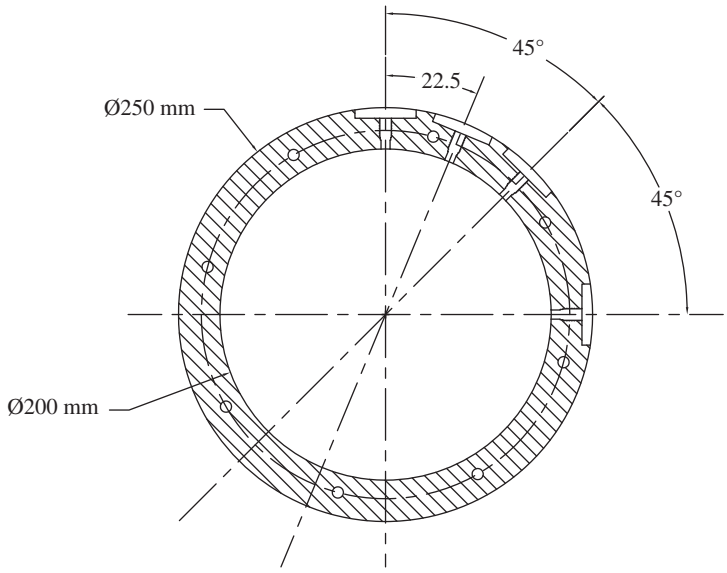

Fig. 3. Locations of the pressure transducers.

The acoustic pressure was measured using piezoelectric type pressure transducers. An acceleration-compensation sensing element was added to the pressure transducer to minimize vibration sensitivity. Four pressure transducers were used to obtain the instantaneous acoustic pressure simultaneously at different physical angles around the circumference of the cavity floor. Fig. 3 shows the relative positions of the pressure transducers. These relative positions were chosen to capture the distribution of the acoustic pressure amplitude.

To determine the characteristics of the approaching boundary layer, a constant temperature hot-wire anemometer (CTA) was used to measure the velocity in the boundary layer at the cavity upstream separation edge. The distributions of both the mean and fluctuation components of the velocity were obtained from the measurements. A DANTEC hot-wire probe type 55P11, mounted on an L-shaped holder and connected to DISA bridge type 56C16 CTA, was used. The hot-wire was traversed across the boundary layer using a traverse mechanism that has a displacement resolution of 20 μm.

Before starting the acoustic pressure measurements, the mean flow velocity was measured for the different blower rotational speed. During the measurement of the acoustic pressure, the Pitot tube was removed and the blower rational speed was gradually varied with a step of 3.33% of the blower maximum speed. For each flow velocity, the amplitude spectrum of each pressure transducer signal, the phase difference and the coherence spectra between the pressure transducers were calculated. Fifty averages of one-second length were used to obtain each spectrum. The data acquisition was performed using a 16-bit 4-channel National Instrument card model PCI-4452, equipped with a built-in anti-aliasing filter. Labview programme was used for acquiring and analysing the signals.

2.3. Test conditions

Acoustic pressure measurements were performed at mean velocities covering the range from 15 to 150 m/s. To characterize the boundary layer at the upstream edge of the cavity, hot-wire measurements were performed at mean velocities of 31, 40, 56.5 and 79 m/s. Fig. 4 shows the radial profile of the normalized mean velocity for 31 m/s. The boundary layer thickness is about 20 mm in this case. For the other measured cases, the data showed a decrease in the boundary layer thickness as the velocity was increased. At 79 m/s, the boundary layer thickness was reduced to about 12 mm. Outside of the boundary layer, the standard deviation of the mean velocity was 0.35%.

Fig. 5 shows the radial distribution of the turbulence intensity, for mean velocity of 31 m/s. The turbulence intensity is normalized by the mean velocity outside the boundary layer. The velocity r.m.s. amplitude outside the boundary layer represents fluctuations in the mean flow rather than turbulence fluctuation. This supposition was verified by comparing simultaneous time signals of the velocity at two different points located outside the boundary layer. The level of the r.m.s. amplitude of the mean flow fluctuations is about 2% of the mean velocity and it appears to be constant at all

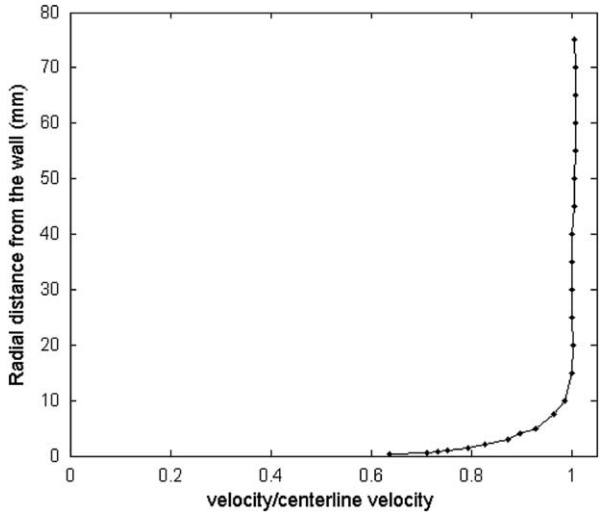

Fig. 4. Radial profile of mean flow velocity at the cavity upstream edge for a reference velocity of 31 m/s at the end of the bell mouth.

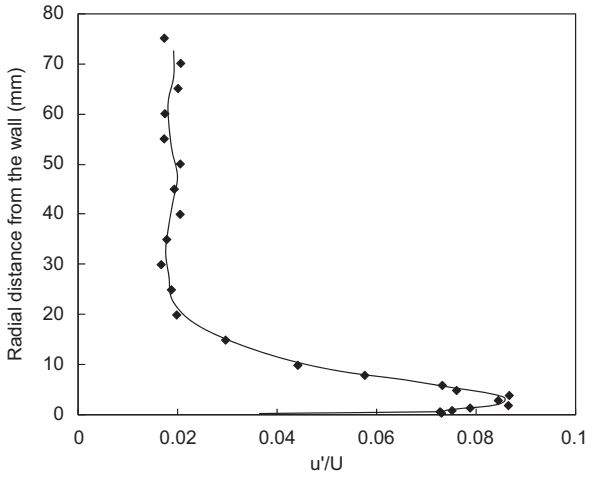

Fig. 5. Radial distribution of the dimensionless r.m.s. amplitude of fluctuation velocity at the cavity upstream edge for a reference velocity of 31 m/s at the end of the bell mouth (the continuous line is a moving average of the measurement data).

measured flow rates. Inside the boundary layer, the turbulence intensity reaches a maximum near 2 mm from the wall. This maximum amplitude decreases monotonically with the increase of the flow rate; it drops from 8.5% at 31 m/s mean velocity to 6.5% at 79 m/s mean velocity.

The displacement and momentum thicknesses were calculated considering a cylindrical coordinate system that has its origin at the pipe centreline. Assuming that the displacement and momentum thicknesses are small compared to the pipe radius, the following expressions can be derived:

$$\delta^* = \int_0^R \left(1 - \frac{u_0(y)}{U}\right)\left(1 - \frac{y}{R}\right) \mathrm{d}y, \tag{1}$$

$$\theta_0 = \int_0^R \frac{u_0(y)}{U}\left(1 - \frac{u_0(y)}{U}\right)\left(1 - \frac{y}{R}\right) \mathrm{d}y, \tag{2}$$

where δ^* is the displacement thickness, y is the distance from the wall, R is the pipe radius, U_0 is the mean velocity and θ is the momentum thickness. The values of the displacement thickness, momentum thickness and the shape factor are

Table 2
List of displacement thickness, momentum thickness and shape factor at different flow velocities.

Average velocity (m/s)	Displacement thickness (mm)	Momentum thickness (mm)	Shape factor
31	1.28	0.92	1.39
40	1.21	0.873	1.38
56.5	1.09	0.834	1.31
79	1.05	0.79	1.33

listed in Table 2 for the various flow velocities. The tabulated data shows that the displacement and momentum thicknesses decrease with the increase of the velocity. Moreover, the shape factor is reasonably constant and approximates the shape factor for the turbulent boundary layer over a flat plate.

3. Characteristics of the diametral modes

Finite element simulations were performed to calculate the frequency and the mode shape of the acoustic resonance modes for different cavity dimensions. The associated acoustic particle velocity fields of the acoustic modes were also calculated using Euler's equation. The results provide the basic characteristics of the diametral modes and they were used to design the experimental set-up and in the analysis of some of the experimental measurements. In the next subsections, details of the finite element approach are presented, followed by the simulation results.

3.1. Simulation of acoustic modes

A finite element commercial package (ABAQUS) was used to predict the frequency and the mode shape of the acoustic resonance at zero flow velocity. This package has a numerical module to extract the natural modes of acoustic enclosures. For the case of zero damping, i.e. no acoustic attenuation within the finite element model, the eigenvalue problem for natural modes of a small amplitude fluctuation can be reduced to the following:

$$(-\omega^2[M]+[K])\{\phi\}=0, \tag{3}$$

where $[M]$ is the mass matrix, $[K]$ is the stiffness matrix, ω is the angular frequency, and $\{\phi\}$ is the eigenvector of the resonance mode. This equation is available directly from a linear perturbation of the equilibrium equation of the system. To calculate the mass and stiffness matrices, the values of both density and the speed of sound were specified to simulate air at room temperature and atmospheric pressure. These values affect only the value of the resonance frequency without having any effect on the mode shape, which depends on the domain geometry and boundary conditions.

A 4-node tetrahedral mesh was used to construct the numerical models. The walls were modelled as solid boundaries with zero pressure gradient. The boundary conditions at each end of the duct were set to zero acoustic pressure (free end) to simulate the open ends with no radiation. Although this may be not the most accurate representation of the physical boundary conditions, the effect of slight deviations from the physical boundary conditions is thought to be small because the modes under consideration are trapped modes with vanishingly small radiation loss as shown by Hein and Koch (2008). Moreover, as will be shown in the next subsection, when the main duct exceeds a certain length, any further increase in the duct length does not affect the mode frequency. In fact, the resonance frequencies calculated from the simulation agree very well with those measured during the experiments. Therefore, the pipe terminations beyond an appropriate length from the cavity can be described as zero pressure boundaries with sufficient accuracy.

3.2. Effect of test-section geometrical parameters on the frequency

The effect of changing the cavity dimensions and the main duct length was investigated by performing a series of simulations of different geometries. In all the simulations, the main duct diameter, D, was kept constant. For a constant main duct length, $\mathscr{L}$, the results of the simulations showed that the frequencies of diametral modes decrease gradually, approaching the cut-off frequency of the cavity section, with the increase of either the cavity length or its depth. In the simulation performed by Hein and Koch (2008), a similar effect of the cavity depth was observed, but the cavity length

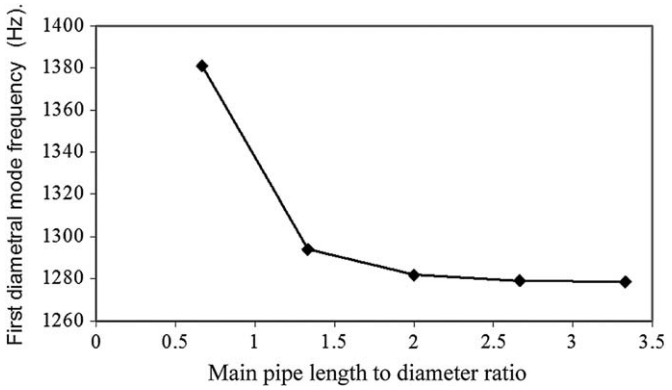

Fig. 6. Variation of the first diametral mode frequency with the main pipe length ($L/d = 1$, $d/D = 2/12$).

did not seem to affect the resonance frequency. This is because the length of the cavity they simulated was rather long ($L/D \geq 1$) such that the mode frequency was almost equal to the cut-off frequency of the cavity section.

The simulation results were used to determine, based on the available maximum flow velocity, the length of the cavity that ensures the excitation of the first 4 diametral modes by the first shear-layer mode of oscillation. This yielded a cavity length of $L = 25\,\text{mm}$ ($L/D = 2/12$) for a cavity depth of $d = 25\,\text{mm}$; resulting in a length to depth ratio of $L/d = 1$, which is the lower limit for shallow cavities.

To determine the effect of the main duct length, the main duct length was changed while the cavity dimensions were kept constant. Fig. 6 shows the change in the first diametral mode frequency as a function of the duct length to diameter ratio, $\mathscr{L}/D$. The plotted data correspond to a cavity with $L/d = 1$ and $d/D = 2/12$. It is seen that the mode frequency is practically uninfluenced by the change in the duct length as long as the length to diameter ratio exceeds a value of 2. For this reason, the ducts used in the experiments were made three diameters long, to ensure that its length has no effect on the shape or the frequency of the diametral modes. Additional simulations were performed for the other cavity geometries. The results showed that a smaller duct length to diameter ratio ($\mathscr{L}/D < 2$) is required to ensure no effect on the mode shape for the cases with larger cavity depth and/or length.

3.3. Characteristics of the mode shapes

This section details the characteristics of the acoustic pressure and particle velocity distributions of the cavity trapped modes. Fig. 7 shows the distribution of the pressure amplitude of the first three diametral acoustic modes for a cavity with $L/d = 1$ and $d/D = 2/12$, which is attached to 450 mm long pipes at both ends ($\mathscr{L}/D = 3$). It is clear from Fig. 7 that the diametral modes are locked to the cavity. Moreover, the higher order modes are more concentrated near the cavity than the lower ones. There are two main characteristics of the acoustic pressure distribution which are of relevance here. First, the maximum acoustic pressure occurs at the cavity floor and midway along its length. Secondly, the acoustic pressure varies in the form of a sine function over the cavity circumference and the number of the complete sine cycles made by the acoustic pressure over the circumference is equal to the mode number, m. This information was useful in selecting the location and the relative position of the pressure transducers as discussed in the previous section and in the analysis of the measurement data.

The distribution of the acoustic particle velocity vector, $\vec{U}_a$, was calculated from the pressure domain, P_a, using Euler's equation:

$$\rho_o = \frac{\partial \vec{U}_a(t)}{\partial t} = -\nabla p_a(t). \tag{4}$$

Consideration of sinusoidal fluctuation of the pressure results in

$$\vec{U}_a = \frac{\nabla p_a}{2\pi f}, \tag{5}$$

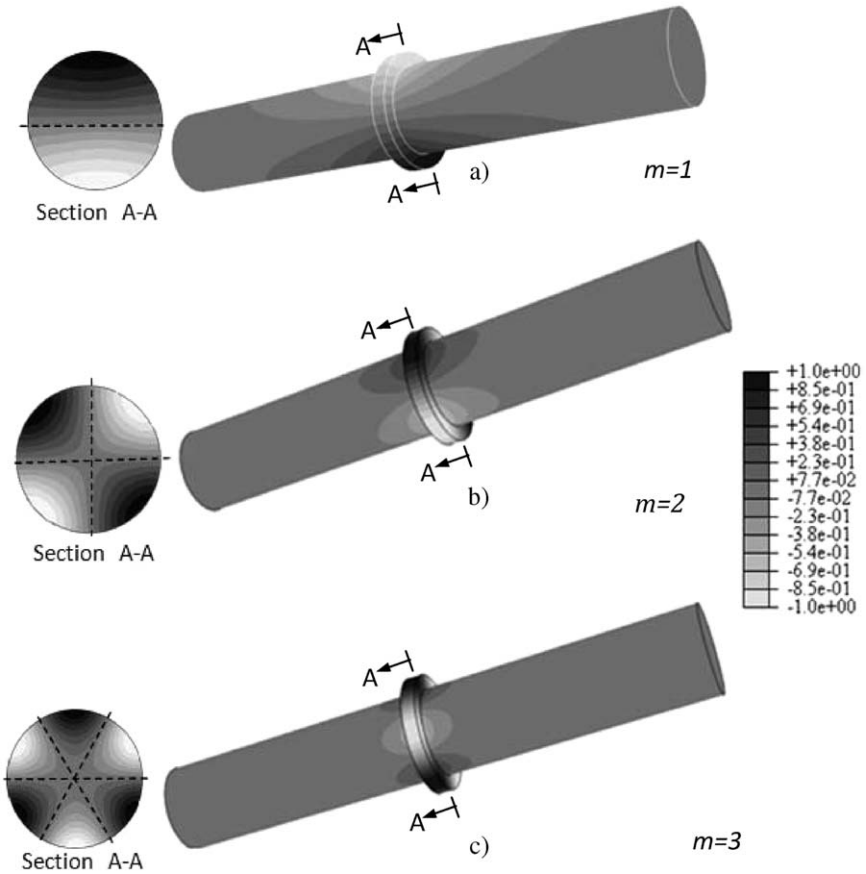

Fig. 7. The mode shapes of the (a) first, (b) second and (c) third acoustic resonance modes. $L/d = 1$ and $d/D = 2/12$.

where ρ_o is the average air density and f is the acoustic resonance frequency. In the current calculation, the density of air is considered 1.2 kg/m^3. The pressure gradient is calculated using a MATLAB programme, the accuracy of which was tested by estimating the particle velocity for simple acoustic mode shapes which have closed-form solutions.

The importance of the acoustic particle velocity in the excitation process has been demonstrated by Howe (1980). He showed that the acoustic power generated by flow vorticity due to its convection in a sound field can be calculated using the following equation:

$$\mathscr{P} = \int \left(\rho \int \vec{\varpi} \cdot \left(\vec{U} \times U_a \right) d\forall \right) \mathrm{d}t, \tag{6}$$

where $\mathscr{P}$ is the power generated, or absorbed, $\vec{\varpi}$ is the vorticity vector and $\vec{U}$ is the instantaneous flow velocity vector. Accordingly, for the diametral modes, the radial component of the particle velocity is the major contributor to the acoustic energy production as it is the component perpendicular to both the mean flow and the free shear-layer vorticity.

Fig. 8 shows vector plots of the acoustic particle velocity over two different cross-sections for the first diametral mode of a cavity with a length and depth of 25 mm ($d/D = 2/12$, $L/d = 1$). Cross-section A-A is the same cross-section as in Fig. 7. The two cross-sections show the planes with the maximum particle velocity. In cross-section A-A, the thin inner circle represents the main pipe circumference which is the edge of the cavity. Fig. 9 shows the contour plots of the radial component of the acoustic particle velocity of the first three diametral modes. The contours are at cross-section A-A of Fig. 7, which is midway along the cavity length. The darkest and brightest areas represent the maximum amplitudes, and are out of phase. The plots show that the areas with maximum radial particle velocity become closer to the cavity floor as the diametral mode number increases. For example, these areas are close to the cavity centreline for the first mode, but are shifted towards the cavity floor for the third mode. At a constant radius, the amplitude changes in the

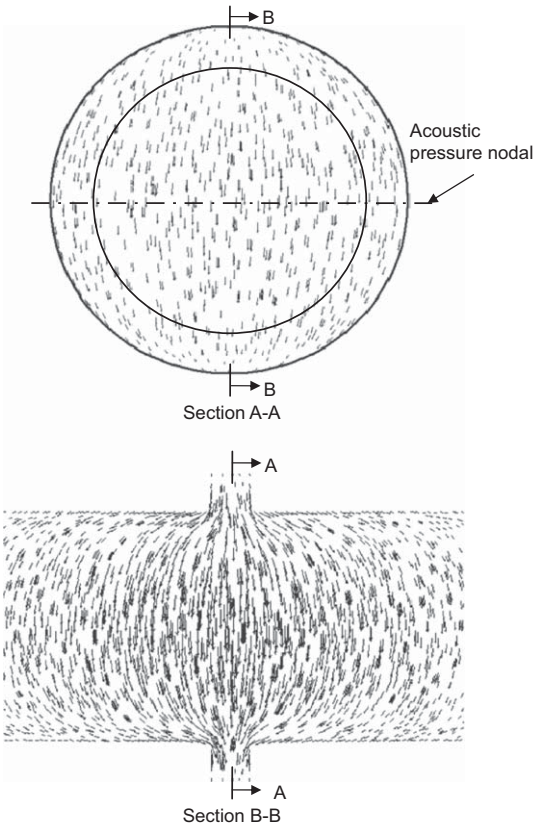

Fig. 8. Vector plots of the acoustic particle velocity amplitude of the first diametral mode ($d/D = 2/12$ and $L/d = 1$).

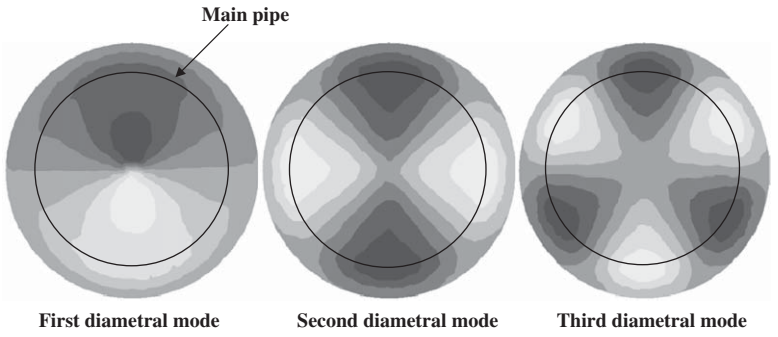

Fig. 9. Contour plots of the radial particle velocity ($d/D = 2/12$ and $L/d = 1$).

form of a sine function in the azimuthal direction similar to the acoustic pressure, and the number of the complete sine cycles made by the velocity amplitude is equal to the mode number.

3.4. *Effect of cavity length on the acoustic particle velocity*

This section focuses on the effect of the cavity length on the particle velocity distribution along the cavity mouth, where the shear-layer oscillation occurs and the acoustic power is generated. The first three diametral modes were simulated for different cavity lengths with the cavity depth kept constant ($d/D = 2/12$).

Fig. 10 shows the amplitude distribution of the first mode acoustic particle velocity over the cavity mouth for $L/d = 1$, 3 and 6. These particle velocity distributions are shown for cross-section B-B in Fig. 8 and correspond to a maximum acoustic pressure of 1 Pa at the centre of the cavity floor. At this cross-section, *the particle velocity is in the radial direction and is at its maximum amplitude*, as can be seen in Figs. 8 and 9. Therefore, these distributions correspond to the *radial component* maximum amplitude. Additional cavities with $L/d = 2$, 4 and 5 were also simulated and the results have shown similar trends. The average amplitudes of the *radial* acoustic particle velocity along the cavity mouth are 1.09, 1.06 and 1.00 mm/s for $L/d = 1$, 3 and 6, respectively. This indicates that the length of the cavity has no major effect on the amplitude of the acoustic particle velocity. The same behaviour was observed for the second and third diametral modes. In the rest of the paper, the average amplitude along the cavity length of the radial particle velocity is used without presenting the complete distribution over the cavity mouth.

3.5. Effect of cavity depth on the acoustic particle velocity

As in the previous section, the focus here is on the effect of the cavity depth on the amplitude of the *radial component* of the acoustic particle velocity over the cavity mouth. The amplitude of the radial component for different cavity depths is shown in Fig. 11 for the first three diametral modes. For these modes, it is evident that the amplitude of the radial particle velocity along the cavity mouth increases with the cavity depth. For example, the particle velocity of the first mode for $d/D = 4/12$ is almost three times higher than that corresponding to $d/D = 1/12$. The change in the acoustic particle velocity amplitude is not linear with the cavity depth. Also, the rate of change is not the same for different acoustic modes. For example, the radial particle velocity component for the third mode reaches a maximum value close to $d/D = 3/12$, while the amplitudes for the first and second modes continue to grow as the cavity gets deeper. This can be clarified by referring again to Fig. 9, where it can be seen that the radial location of the particle velocity maximum amplitude depends on the mode order.

3.6. Radiation losses

The level of acoustic power radiation from the pipe terminations depends on the shape of the resonance mode and on the pressure amplitude at the pipe terminations. As mentioned in the Introduction, the pressure amplitude of the diametral modes decays exponentially along the main pipe further away from the cavity. The rate of this decay depends on the ratio of the frequency of the diametral mode to the cut-off frequency of the main duct (Kinsler et al., 2000). Therefore, since the frequency of the diametral mode is controlled by the cavity dimensions, the cavity dimensions control the rate of the pressure decay and consequently the relative pressure amplitude at the pipe ends in comparison to the pressure amplitude at the cavity floor.

Fig. 12 shows the pressure decay with axial distance from the cavity centre. The decay distributions are obtained from the results of the finite element simulations of the acoustic modes for different cavity dimensions. The acoustic pressure seems to decay faster with the increase of either the cavity depth or length. For the cavity with $L/d = 2$ and $d/D = 1/12$, the pressure amplitude of the first diametral mode at the pipe end is about 20% of the amplitude at the cavity floor, but for the cavity with $L/d = 1$ and $d/D = 2/12$, it is about 2.5% and for the cavity with $L/d = 4$ and $d/D = 1/12$, it is about 7%. This indicates the relative increase in the acoustic radiation losses from the pipe ends as the cavity gets shorter or shallower (i.e. as its size becomes smaller). The figure shows also that the amplitude of the second diametral mode decays much faster than the amplitude of the first diametral mode, and the rate of decay of the third diametral mode seems to be even higher. These results illustrate the fact that the rate of acoustic power radiation decreases with the increase of the order of the diametral mode.

4. Overview of the acoustic response

Before discussing the effect of changing the cavity dimensions on the excitation of the diametral modes, it is important to illustrate the main characteristics of the excitation mechanism. For this purpose, the test results of a base case configuration will be first presented in some detail. Thereafter, the results of the other cases are discussed briefly. The cavity of the base configuration is 25 mm deep and 25 mm long ($L/d = 1$, $d/D = 2/12$).

Generally, for each of the tested cavities, a number of acoustic pressure spectra were recorded for different flow velocities up to the highest capacity of the blower. To gain overall perspective of the system behaviour, these acoustic pressure spectra are presented together in the form of a three-dimensional waterfall plots, as shown in Fig. 13. These are simply isometric views of pressure spectra including grey scale contours for the r.m.s. acoustic pressure. The spectral

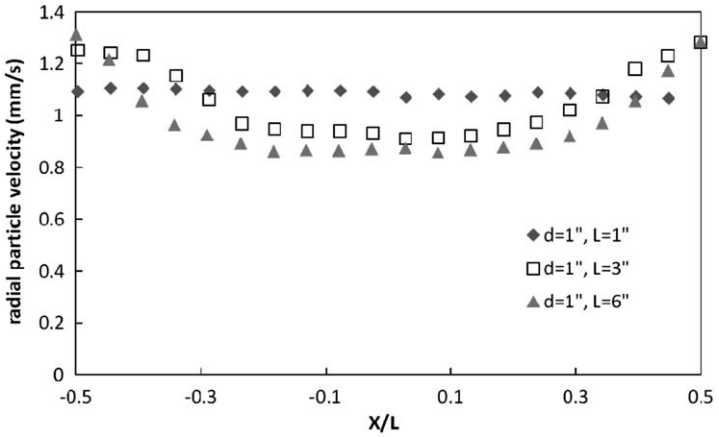

Fig. 10. Radial component of the acoustic particle velocity along the cavity mouth corresponding to acoustic pressure of 1 Pa at the centre of the cavity floor ($d/D = 2/12$).

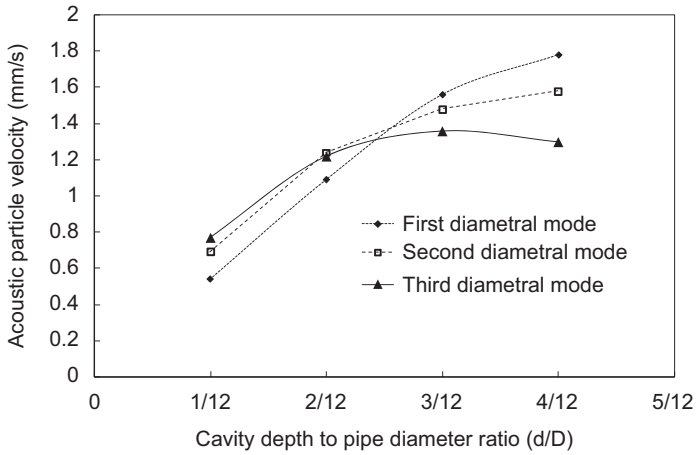

Fig. 11. Maximum radial acoustic particle velocity for different d/D ratios. The data corresponds to acoustic pressure of 1 Pa at the center of the cavity floor ($L/D = 2/12$).

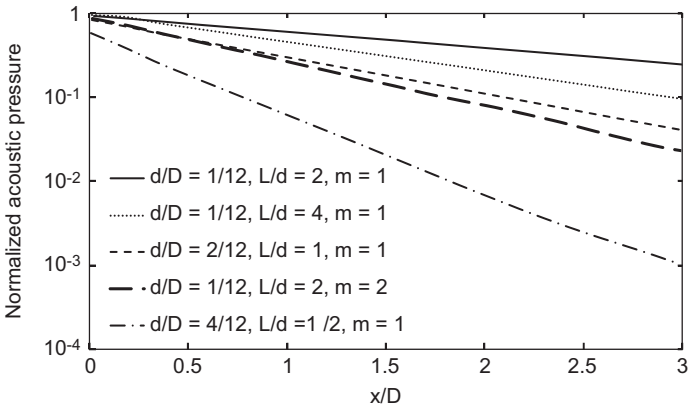

Fig. 12. Axial distribution of acoustic pressure decay for various cavity dimensions; m is the acoustic mode order and x is measured from the cavity centre.

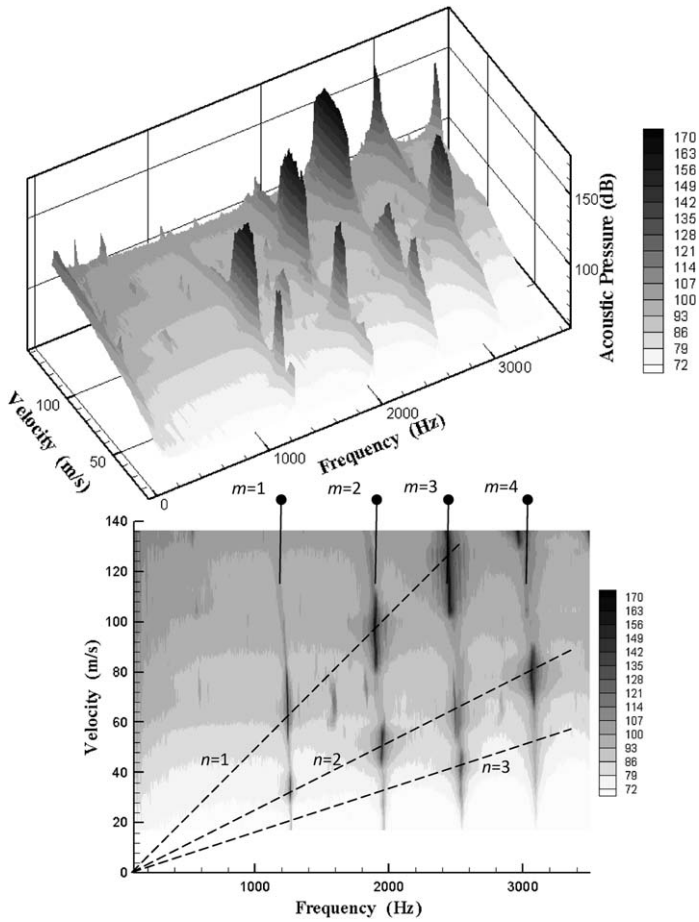

Fig. 13. Waterfall plot and 2-D pressure contours for $L/d = 1$, $d/D = 2/12$; m is the diametral mode number, and n is the free shear-layer mode number.

peaks, therefore, appear darker than the rest of the spectra. The acoustic pressure scale has a maximum of 170 dB and a minimum of 60 dB. The logarithmic scale is used to help illustrate the relatively low amplitude peaks beside the dominant ones on the same graph. Two-dimensional top views of the pressure contours, in the velocity versus frequency plane, are also provided below each isometric view. These views illustrate the velocities at which different acoustic resonance modes are excited. This representation will be used for all tested cases to illustrate the aeroacoustic response of the cavity–duct system.

The spectra in Fig. 13 correspond to a velocity range from 15 m/s to about 140 m/s. The first four acoustic diametral resonance modes ($m = 1$–4) are strongly excited. The maximum sound pressure level measured during these tests reached about 172.5 dB (8.5 kPa). The frequencies of these resonance modes agree well with the values obtained from the finite element simulation. For example, the measured first mode frequency at a mean flow velocity of 30 m/s is 1269 Hz, while the calculated one is 1280 Hz. However, the acoustic resonance frequencies of the different modes seem to decrease slightly with the flow velocity. Koch (1983) reported a similar frequency reduction with the Mach number for the trapped modes of a cascade arrangement.

Scrutiny of the overall acoustic response shown in Fig. 13 indicates that the cavity–duct system is very susceptible to flow-excited acoustic resonances and that its acoustic response is dominated by the resonance of the diametral modes, such that at least one mode is excited at any flow velocity above 30 m/s. Simultaneous excitation of two acoustic modes was also observed during the experiments. However, in most cases, the different modes were excited alternately in time. Moreover, the plots show a weak excitation of some purely longitudinal modes and some diametral–longitudinal combined modes.

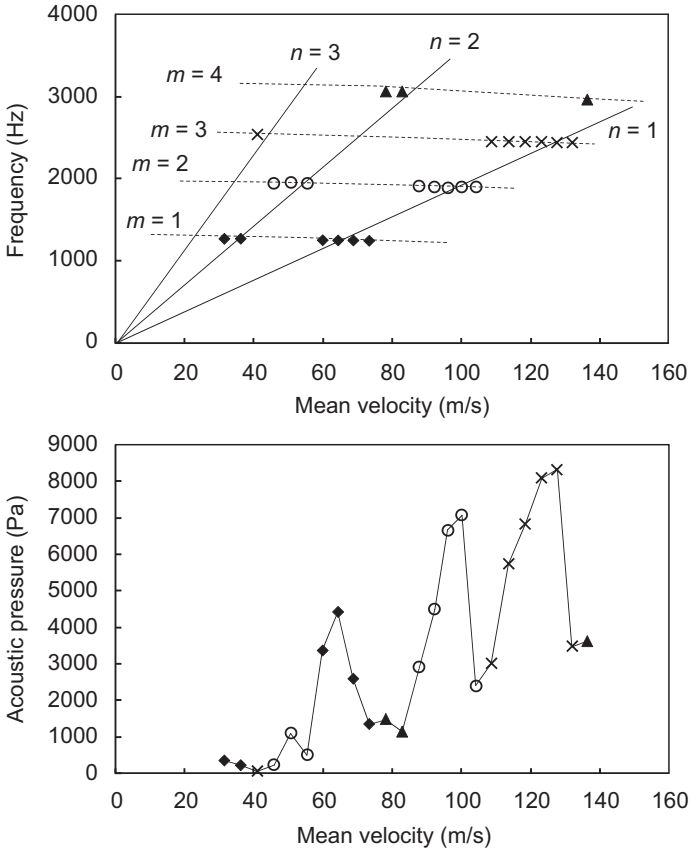

Fig. 14. Frequencies and amplitudes of the dominant acoustic modes as function of flow velocity ($L/d = 1$, $d/D = 2/12$); m is the diametral mode number, n is the free shear-layer mode number.

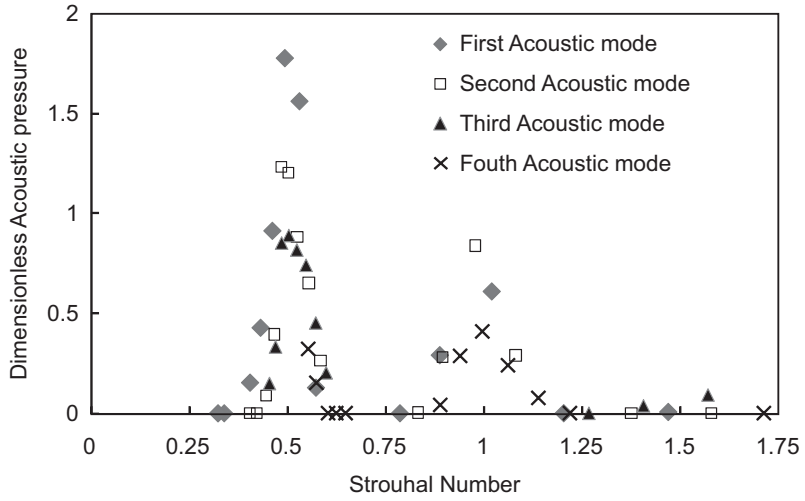

Fig. 15. Dimensionless acoustic pressure as function of the Strouhal number ($L/d = 1$, $d/D = 2/12$).

Referring again to Fig. 13, each acoustic mode ($m = 1$–4) is seen to be excited over multiple ranges of flow velocity. These ranges correspond to specific Strouhal numbers associated with three different instability modes of the cavity shear-layer oscillations ($n = 1$–3). However, the pressure spectra show no sign of organized shear-layer oscillations

other than those resulting from acoustic resonance. Fig. 14(a) shows the frequencies of the dominant acoustic modes as a function of the flow velocity. The data show upward and downward frequency jumps, from one acoustic mode to another, as the velocity increases. This behaviour exemplifies the general trend of cavity-excited acoustic resonance as reported in the literature, for example, by Schachenmann and Rockwell (1980). In general, the first and second free shear-layer modes ($n = 1, 2$) excite the first four diametral modes ($m = 1$–4), alternately. However, the third free shear-layer mode ($n = 3$) excites the second and third diametral modes over very narrow velocity ranges. Fig. 14(b) shows the acoustic pressure amplitude of the dominant modes as a function of the flow velocity. Pronounced acoustic resonances start to appear in the pressure spectra above a mean flow velocity of $U \approx 30$ m/s, which corresponds to a Mach number of approximately 0.09. At higher flow velocities, the amplitude goes up and down over each lock-in region, with the mean amplitude rising as the velocity increases.

Fig. 15 shows the dimensionless pressure amplitude of the excited modes as a function of the Strouhal number of each mode while it is excited. The dimensionless pressure amplitude is the r.m.s. acoustic pressure normalized by the dynamic head of the mean flow ($\frac{1}{2}\rho U^2$). The Strouhal number, fL/U, is based on the cavity length, L, the resonance mode frequency, f, and the mean flow velocity, U. The first mode of the free shear-layer instability, $n = 1$, excites the acoustic modes over a Strouhal number range from 0.4 to 0.6. The maximum acoustic pressure over this range occurs at a Strouhal number close to 0.5. Following a similar trend, the second cavity free shear-layer mode, $n = 2$, generates resonance over a Strouhal number range from 0.8 to 1.15, and the maximum amplitude occurs at a Strouhal number near 1. The third cavity free shear-layer mode, $n = 3$, is observed to excite the third diametral mode only weakly over a narrow velocity range near 41 m/s, which corresponds to a Strouhal number of 1.55. It is noticeable that these Strouhal numbers remain virtually constant for different acoustic resonance modes, which differs from the Strouhal number of the fluid-dynamic oscillations that decreases with the increase of the Mach number (Tam and Block, 1978). Regarding the resonance intensity, the first free shear-layer mode is seen in Fig. 15 to generate the strongest acoustic resonances, reaching a dimensionless amplitude of 1.8, whereas the highest dimensionless amplitude excited by the second shear-layer mode is about 0.9, and that excited by the third shear-layer mode is less than 0.1. For the excitation by a certain free shear-layer mode, the *dimensionless* amplitude at resonance decreases with the flow velocity and consequently as the order of the diametral mode increases. This later observation should be considered with care because although the dimensionless amplitude of higher order modes may be smaller, the absolute value of pressure pulsation may be higher because the pulsation amplitude scales with the square of the flow velocity.

5. Effect of cavity length

This section discusses the effect of changing the cavity length on the acoustic response of the cavity–duct system, while maintaining the cavity depth constant at 25 mm ($d/D = 2/12$). First, the change in the general behaviour of the aeroacoustic response is discussed based on the waterfall plots and the 2-D pressure contours. Thereafter, the effect of the cavity length on the acoustic pressure amplitude at resonance is examined.

5.1. Effect of cavity length on the general acoustic response

Figs. 16–20 show the waterfall plots and the 2-D contours of the r.m.s. acoustic pressure for $L/d = 2$–6. Straight lines are drawn on each 2-D plot to indicate the shear-layer modes. The diametral modes are also marked for visual aid. The unmarked peaks correspond to either higher harmonics of excited diametral modes or longitudinal and combined modes. As a general observation not related to the acoustic resonance mechanism, the available maximum flow velocity during the tests decreases with the increase of the cavity length because the flow resistance of the cavity–duct system increases when the cavity is made longer.

Starting with the data of the cavity with $L/d = 2$, shown in Fig. 16, the behaviour of this case is very similar to the cavity with $L/d = 1$, which is discussed in the previous section. The change of cavity length alters the velocity ranges over which the acoustic modes are excited. It is noteworthy that, in these two cases, the longitudinal acoustic modes of the pipe have not been excited during the tests. Regarding the resonance frequencies, the increase of the cavity length from $L = 25$ mm ($L/d = 1$, $d/D = 2/12$) to $L = 50$ mm ($L/d = 2$, $d/D = 2/12$) results in a drop in the diametral mode frequencies by about 5% from the case of $L/d = 1$. This is consistent with the finite element results and indicates that the boundary conditions used in the simulation are satisfactory. For both cases with $L/d = 1$ and 2, the measured resonance frequencies decrease slightly with the increase of the mean flow velocity. This observation is more pronounced for the lower diametral modes; though, when the first diametral mode is excited by the second free shear-layer mode, the frequency appears to be more or less constant or experience a very slight increase.

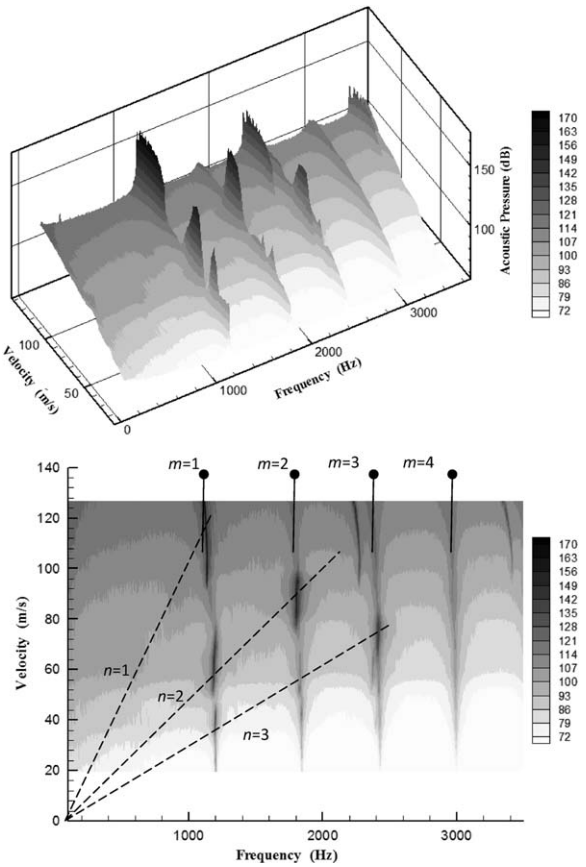

Fig. 16. Waterfall plot and 2-D pressure contours for $L/d = 2$, $d/D = 2/12$; m is the diametral mode number, n is the free shear-layer mode number.

The results of the cavity with $L/d = 3$ are shown in Fig. 17. This geometry is able to excite the diametral modes strongly with second, third and fourth shear-layer modes. However, the level of pressure amplitude is lower than the amplitude level in the previous two cases ($L/d = 1$, 2). In this case, longitudinal modes are also excited, but exhibiting extremely small amplitude. At 95 m/s, the second free shear-layer mode shifts from exciting the first diametral mode to exciting a longitudinal mode that has a frequency just about 10 Hz higher than the diametral mode frequency. According to the finite element simulation, this longitudinal mode has a pressure antinode near the middle of the cavity length, which explains its relative strong appearance in the waterfall plot. However, this longitudinal mode has a relatively lower amplitude than the diametral modes which is to be expected due to its high level of radiation losses.

Longer cavities ($L/d = 4$–6), shown in Figs. 18–20, are also capable of exciting the diametral modes, even with the fourth shear-layer mode; but, the pressure amplitude decreases consistently with the length. Re-examining the aeroacoustic response of different cavities shows that the essential feature which distinguishes long cavities ($L/d = 3$–6) from short ones ($L/d = 1$–2) is the appearance of small spectral peaks indicating that the pipe longitudinal modes can also be excited in the case of the longer cavities. The spectral peaks of the longitudinal modes follow constant Strouhal number lines. This is more noticeable at frequencies lower than the first diametral mode frequency. In this context, it should be re-emphasised that it is not appropriate to compare the amplitudes of the longitudinal modes with those of the diametral modes. However, it is clear that the level of the pressure amplitude of the longitudinal modes and the number of the longitudinal modes being excited show consistent increase with the increase of the cavity length. They start as very few and faint traces in the waterfall plot for $L/d = 3$ in Fig. 17, and continue to gain strength as the cavity length increases until they are continually excited over most of the velocity range for the cavity with $L/d = 6$, as shown in Fig. 20. However, the longitudinal modes seem to subside as soon as one of the diametral modes is excited. This can be seen in Fig. 18 for a cavity length of $L/d = 4$ at 68 m/s, and also in Fig. 19 for a cavity length of $L/d = 5$ at 80 m/s,

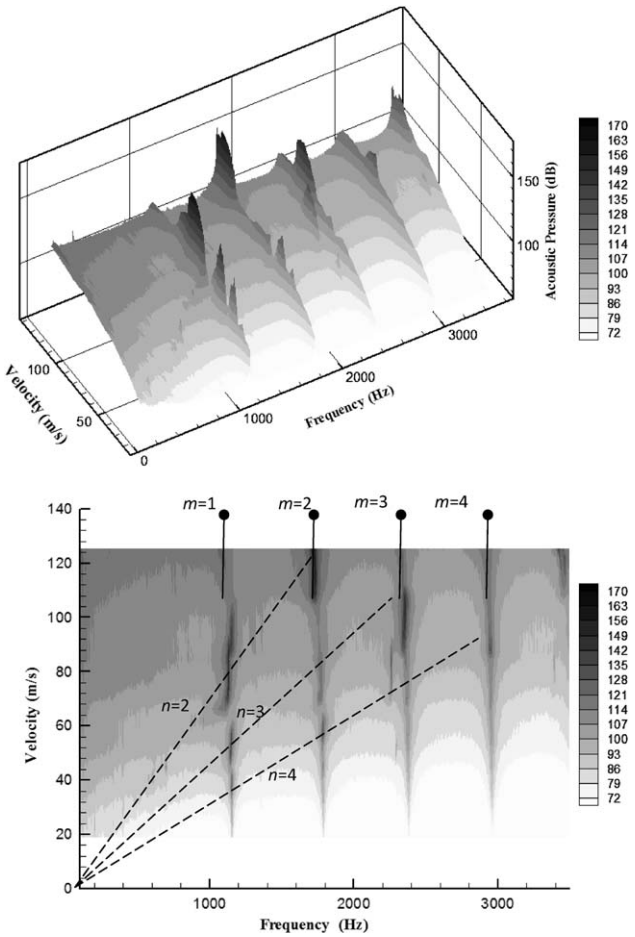

Fig. 17. Waterfall plot and 2-D pressure contours for $L/d = 3$, $d/D = 2/12$; m is the diametral mode number, n is the free shear-layer mode number.

where the first diametral mode is excited by the third shear-layer mode in both cases. Moreover, the diametral and the longitudinal modes are not excited simultaneously, but rather alternately.

5.2. *Effect of cavity length on the pressure amplitude*

The discussion in this section aims to quantify the reduction in the acoustic pressure amplitude due to the increase of the cavity length and also to highlight some of the physics behind this trend. Fig. 21 shows the maximum dimensionless amplitudes occurring at different free shear-layer modes for all cavity lengths. In this figure, "n" is the cavity free shear-layer mode number and "m" is the diametral mode order. These data points are extracted from the graphs of the dimensionless pressure versus the Strouhal number, which are similar to that shown in Fig. 15. All data points correspond to the first diametral mode. Due to the limited capacity of the wind tunnel, the low order shear-layer modes ($n = 1$, 2) did not excite the first acoustic mode for the cases of long cavities. This limits the number of data points available for $n = 1$, 2. The dimensionless pressure decreases by an order of magnitude as the cavity length to pipe diameter ratio, L/D, increases from 1/6 to 1. Also, it is clear that the pressure amplitude decreases with the increase of the order of the free shear-layer mode. This decrease may be attributed to the reduction of both the size and the fluctuation velocity of the shear-layer vortical structures with the increase of the shear-layer mode order for constant cavity length. Scrutiny of Fig. 21 shows that the resonance amplitude caused by the second, third and fourth shear-layer modes increases with the cavity length at the beginning then starts decreasing after a certain length. This length varies from one shear-layer mode to another. An identical trend is observed for the other tested cavity depths ($d/D = 4/12$ and

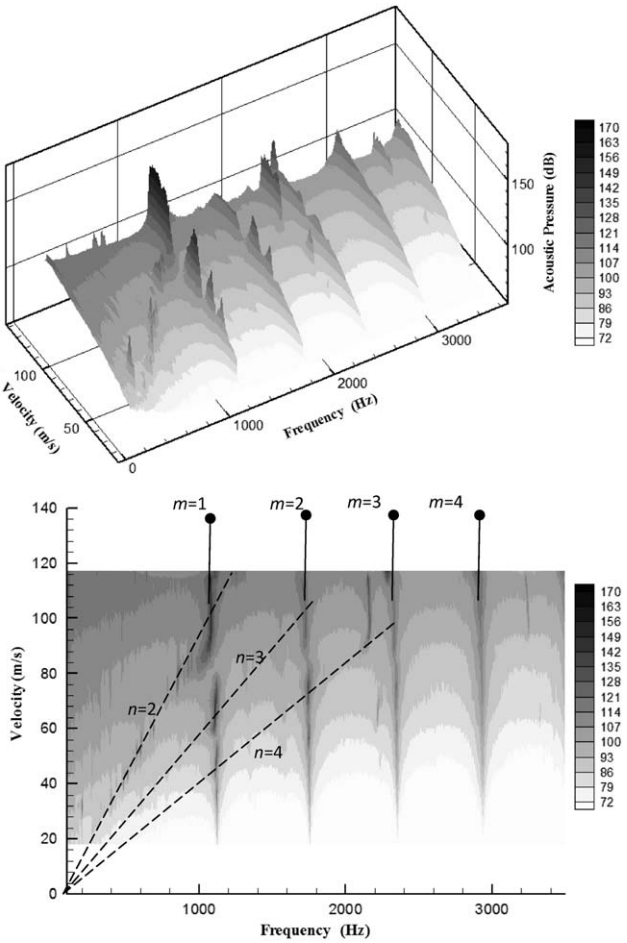

Fig. 18. Waterfall plot and 2-D pressure contours for $L/d = 4$, $d/D = 2/12$; m is the diametral mode number, n is the free shear-layer mode number.

1/12). Therefore, it can be concluded that this trend is independent of both the cavity depth and the cavity length to depth ratio.

To examine the effect of the mean flow velocity, the same data are plotted against the mean flow Mach number in Fig. 22. Data corresponding to the excitation of the second and third diametral modes is added to broaden the comparison. The dimensionless pressure amplitude increases with the mean Mach number until it reaches a Mach number between 0.15 and 0.2. Thereafter, the amplitude decreases with further increases in the Mach number. All free shear-layer modes follow this same trend. Plotting the dimensionless pressure amplitude against the Mach number shows more clearly the drop of the maximum resonance amplitude as the order of the free shear-layer increases. In Fig. 22, the data corresponding to the different diametral modes ($m = 1$, 2 and 3) aligns together depending on the shear-layer mode. This improves the confidence in the generality of the current normalization parameters. However, it appears that the dimensionless pressure amplitude also decreases with the increase of the order of the diametral modes, especially in the case of the second free shear-layer mode ($n = 2$).

6. Effect of cavity depth

Two cavity depths ($d = 12.5$ and 50 mm) were investigated in addition to the one studied in the previous section ($d = 25$ mm) to determine the effect of the cavity depth, with respect to the pipe diameter (D), on the acoustic response

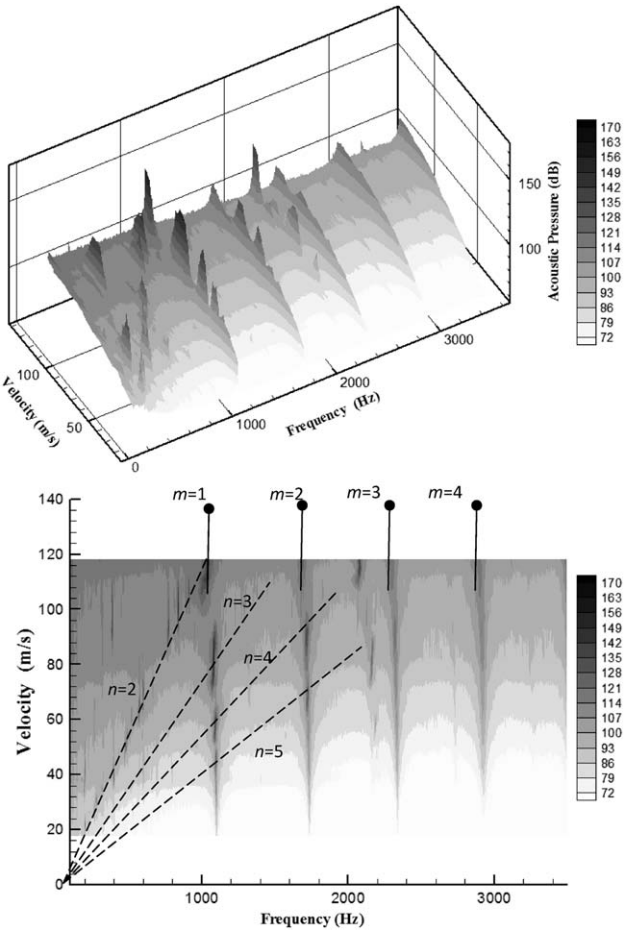

Fig. 19. Waterfall plot and 2-D pressure contours for $L/d = 5$, $d/D = 2/12$; m is the diametral mode number, n is the free shear-layer mode number.

of the cavity–duct system. For each depth, the cavity length was changed from 25 to 150 mm in steps of 25 mm. For $d = 12.5$ mm ($d/D = 1/12$), the maximum cavity length to depth ratio is $L/d = 12$. This L/d ratio is classified as a closed cavity, for which the free shear layer reattaches to the cavity floor. On the other hand, for $d = 50$ mm ($d/D = 4/12$), the minimum L/d is 0.5, which is classified as a deep cavity. Those two extremes demonstrate the wide range of cavity aspect ratios investigated in this section.

6.1. *Effect of cavity depth on the general acoustic response*

Figs. 23–26 show the waterfall plots and the 2-D pressure contours of the RMS acoustic pressure for cavities with $L/d = 2$, $d/D = 1/12$; $L/d = 6$, $d/D = 1/12$; $L/d = 1/2$, $d/D = 4/12$ and $L/d = 3/2$, $d/D = 4/12$, respectively. In Fig. 23, the contour plot for the cavity with $L/d = 2$ and $d/D = 1/12$ shows that the first four diametral modes are excited. Each mode is excited over different velocity ranges by the first and second shear-layer modes. The excitation of the diametral modes by the third shear-layer mode is rather weak. This behaviour is similar to that of the cavity with $L/d = 1$ and $d/D = 2/12$ (Fig. 13). The sound pressure level for cavities with $d/D = 1/12$ is generally lower than the sound pressure level for cavities with $d/D = 2/12$, as can be seen from comparing Figs. 23 and 13. Fig. 27 shows the dimensionless amplitude of the diametral modes versus the Strouhal number for the cavity shown in Fig. 23 with $L/d = 2$, $d/D = 1/12$. The Strouhal numbers of the first and second free shear-layer modes are about 0.44 and 0.88, respectively. This indicates a drop in the convection speed of the free shear-layer vortex in comparison to the cavities with $d/D = 2/12$.

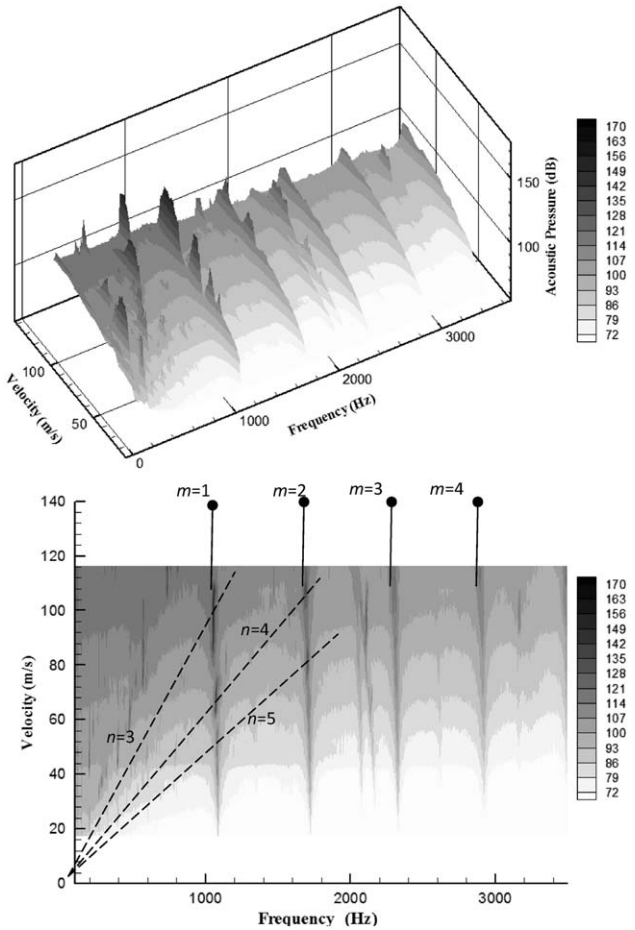

Fig. 20. Waterfall plot and 2-D pressure contours for $L/d = 6$, $d/D = 2/12$; m is the diametral mode number, n is the free shear-layer mode number.

Regarding the pressure amplitude, the maximum dimensionless pressure of the first diametral mode is about 0.1 when it is excited by the first free shear-layer mode. This is about 20 times lower than the maximum amplitude for the cavity with $L/d = 1$, $d/D = 2/12$ (Fig. 15). For the second diametral mode, the dimensionless amplitude decreases by a factor of 4 with the decrease of the cavity depth. Moreover, the decrease in the amplitudes of the third and fourth diametral modes is of the same order as the second diametral mode or less. This indicates that the effect of changing the cavity depth depends on the mode order. This phenomenon is further investigated in Section 8.

For the third depth studied ($d/D = 4/12$), all the cases exhibit very high level of acoustic pressure. Fig. 25 shows the waterfall and the 2-D contour plots for the cavity with $L/d = 1/2$ and $d/D = 4/12$. This case has length to depth ratio of 0.5, which makes it a deep cavity. However, the system behaviour is very similar to that of the other cavities. In this case, the first three diametral modes are strongly excited. Also, some of the longitudinal modes are excited. The amplitude of the second diametral resonance mode reaches 35 kPa at a mean flow velocity of 107 m/s. This amplitude is about 40% of the mean static pressure of the system. During the strong excitation of the first and second diametral modes, the system resistance increases substantially such that the rate of increase of the mean flow rate with the blower rotational speed drops by 35–40% of the average rate. These results indicate the significant effect of acoustic resonance in altering the operating conditions of the system.

Fig. 28 shows the dimensionless amplitude of the acoustic pressure as a function of Strouhal number for the cavity shown in Fig. 25 with $L/d = 1/2$ and $d/D = 4/12$. The maximum dimensionless amplitude is about 4.3 and it occurs at a Strouhal number of 0.35, where the first free shear-layer mode excites the first diametral mode. The second and third diametral modes reach dimensionless amplitudes of 3.6 and 1, respectively. The Strouhal number of the second free shear-layer is about 0.8 with a maximum dimensionless amplitude of 1.25. Fig. 26 shows the waterfall and the 2-D

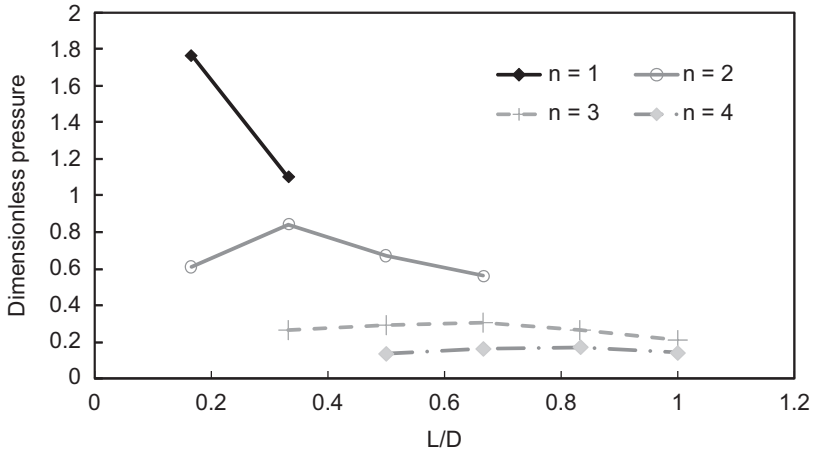

Fig. 21. Effect of cavity length on the maximum dimensionless pressure for the first diametral mode (n: the free shear-layer mode number; the lines are for visual aid only).

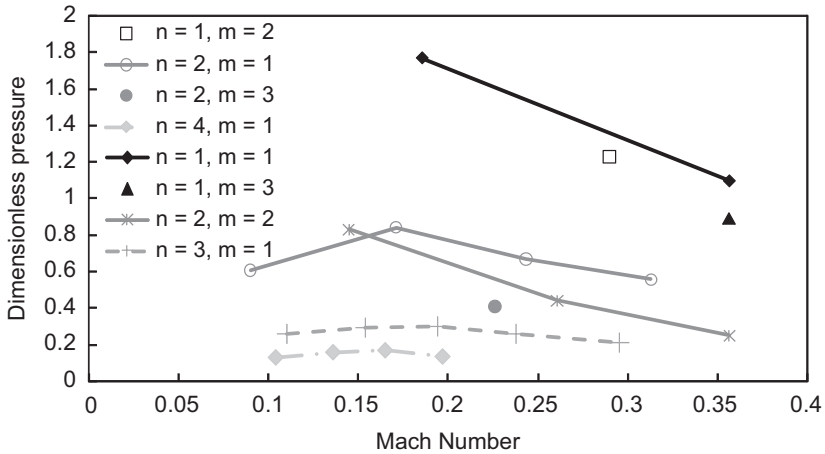

Fig. 22. Effect of Mach number on the maximum dimensionless pressure for the different free shear-layer modes (m: the acoustic mode number, n: the free shear-layer mode number).

contour plots for the cavity with $L/d = 3/2$ and $d/D = 4/12$. Comparing Figs. 26 and 17 shows that the overall behaviour of the 50 mm depth cases is very similar to the 25 mm depth cases. It is worth mentioning that the high order diametral modes ($m = 3, 4$) experience a lower level of amplification compared to the lower order ones ($m = 1, 2$). This trend is discussed in detail in Section 8.

6.2. *Effect of cavity depth on the pressure amplitude*

As illustrated in the previous section, the amplitude of the acoustic pressure is strongly influenced by the cavity depth or, in other words, by the cavity depth to the pipe diameter ratio (d/D). Fig. 29 shows the maximum dimensionless acoustic pressure of the lowest diametral mode ($m = 1$) when excited by the first shear-layer mode (Fig. 29(a)) and by the second shear-layer mode (Fig. 29(b)). The results are given for the three tested cavity depths (d/D), and the cavity length is taken as a parameter. It is evident that the ratio d/D has a strong effect on the excitation level of the diametral acoustic modes. The plots depict the trend of the change in the pressure amplitude with the cavity depth to pipe diameter ratio. This trend indicates that a further decrease in the cavity depth may suppress the diametral mode resonance altogether. Based on the available results, the suppression of the diametral mode resonance is likely to occur

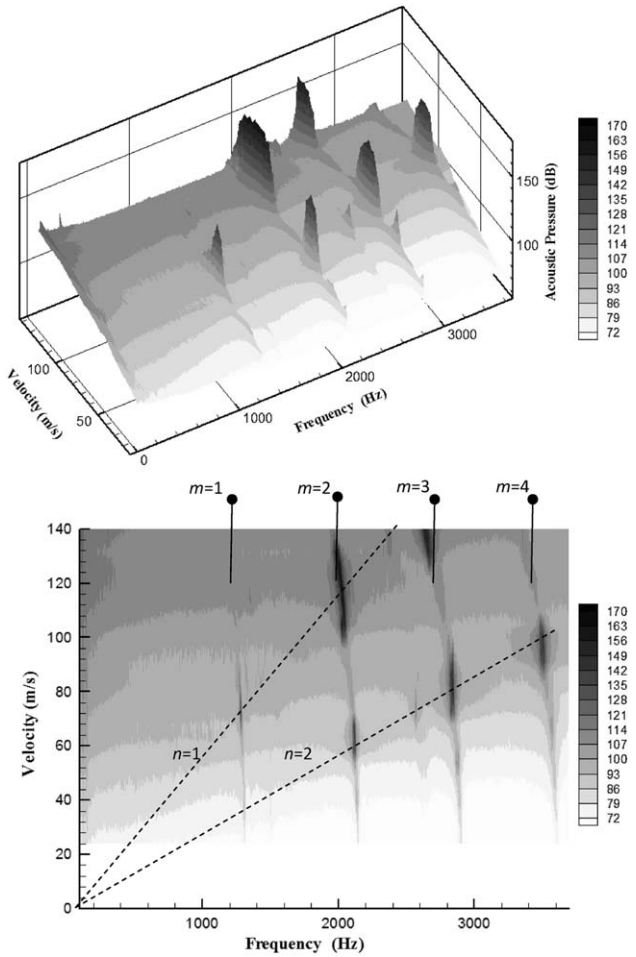

Fig. 23. Waterfall plot and 2-D pressure contours for $L/d = 2$, $d/D = 1/12$; m is the diametral mode number, n is the free shear-layer mode number.

for a cavity depth as small as $d/D < 5\%$. This indicates how small the cavity depth needs to be to alleviate the resonance of the diametral acoustic modes. The trend discussed above seems to be independent of the cavity length or the cavity free shear-layer mode.

Referring to the discussion in Section 3.5, it is clear that the increase in the acoustic pressure with increase of the cavity depth is essentially a result of the consequent increase of the acoustic particle velocity (Fig. 11), which increases the rate of acoustic power generation in the shear-layer region (Howe, 1980). Also, increasing the cavity depth reduces the resonance frequency far below the cut-off frequency of the main duct (Hein and Koch, 2008) and consequently the diametral mode becomes more contained inside the cavity. This causes the rate of acoustic radiation from the duct terminations to decrease with the increase in the ratio of the cavity depth to pipe diameter (Fig. 12). The effect of reducing the acoustic radiation is similar to the effect of increasing the particle velocity on the generation of higher pressure amplitudes.

6.3. *Effect of cavity depth on excitation of longitudinal modes*

Longitudinal modes, as described before, are one-dimensional, standing plane waves which extend along the main duct and are not combined with diametral modes. These modes are therefore distinguished from the cross- (or diametral) modes and from the combined diametral–longitudinal modes. The frequencies of the longitudinal modes are generally lower than those of the diametral and the combined modes. The excitation of these longitudinal modes was

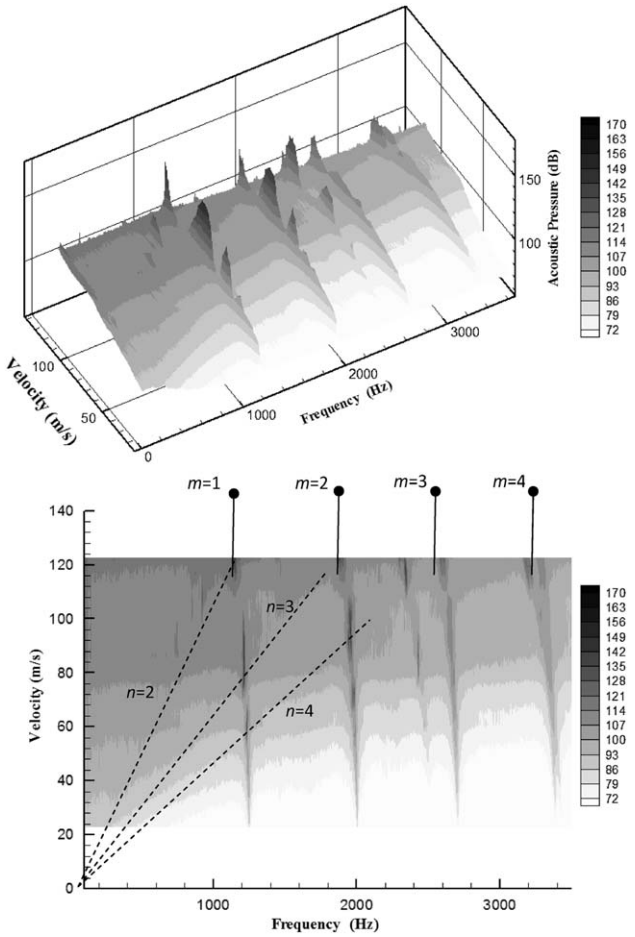

Fig. 24. Waterfall plot and 2-D pressure contours for $L/d = 6$, $d/D = 1/12$; m is the diametral mode number, n is the free shear-layer mode number.

evident for the three tested depths when the cavity length to pipe diameter ratio was increased to 1/2 or larger (Figs. 17, 24 and 26). For all cavity depths, the excitation level increases with the cavity length as described in Section 5. However, the level of excitation increases with the increase in the ratio of the cavity depth to pipe diameter. For $d/D = 1/12$, the longitudinal modes did not dominate the system behaviour *for long cavities* as in the other two cases with $d/D = 2/12$ and 4/12. It should be noted however that the acoustic resonance of the longitudinal modes is outside the scope of the present investigation because the pressure transducers were positioned at a single streamwise location. For further details on this topic, the reader is referred to earlier work in the literature [e.g. Rockwell et al. (2003)].

7. Strouhal number of cavity resonance

To examine the effect of the cavity length on the Strouhal number and the pressure amplitude, a series of plots similar to Figs. 15, 27 and 28 depicting dimensionless amplitude against the Strouhal number of the acoustic resonance were constructed for all tested cases. For all excited modes, the dimensionless pressure amplitude exhibits clear resonance peaks over different ranges of Strouhal number that correspond to different cavity free shear-layer modes. The Strouhal number at the peak of each resonance is considered to be the fluid resonance Strouhal number of the corresponding free shear-layer mode.

Fig. 30 shows the Strouhal numbers of the cavity free shear-layer modes for all the studied cases. Generally, the Strouhal number seems to change with the cavity length to depth ratio (L/d), which controls the flow field inside the

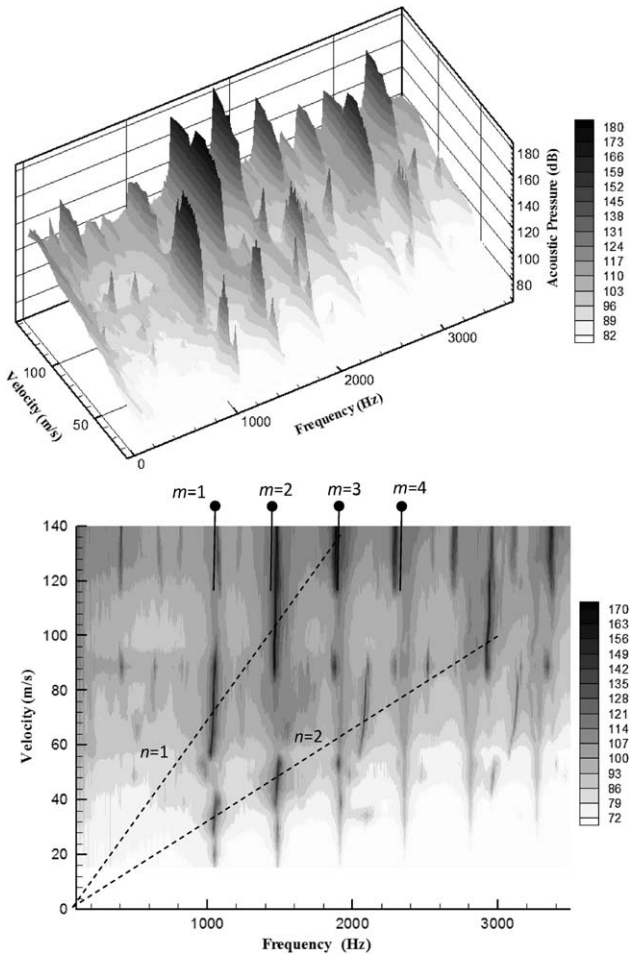

Fig. 25. Waterfall plot and 2-D pressure contours for $L/d = 0.5$, $d/D = 4/12$; m is the diametral mode number, n is the free shear-layer mode number.

cavity. For small L/d, less than two, the Strouhal number increases with the cavity length. However, for L/d greater than four, the Strouhal number seems to decrease slightly with the cavity length. On the other hand, the cavity depth to pipe diameter ratio does not seem to have a significant effect on the Strouhal number. The data for the three different depths match relatively well. However, the data of $d/D = 1/12$ is slightly lower, which could be attributed to the effect of the ratio of the depth to the momentum thickness, which is about 15 at a flow velocity of 70 m/s.

8. Mode selectivity

The general behaviour of the excitation of the diametral modes can be described in terms of the velocity ranges over each of which certain shear-layer modes can excite certain diametral modes. These velocity ranges depend on both the cavity length and the pipe diameter. The cavity length determines the shear-layer oscillation frequency for a given flow velocity and the pipe diameter determines the frequencies of the diametral modes. Thus, in general, the ratio of cavity length over the pipe diameter (L/D) dictates the aeroacoustic response of the cavity–duct system. This means that two different cavity–duct systems with the same L/D will have a similar acoustic response. Also, it should be kept in mind that the aspect ratio of the cavity (L/d) slightly affects the Strouhal number, and the cavity size alters the frequencies of the diametral modes.

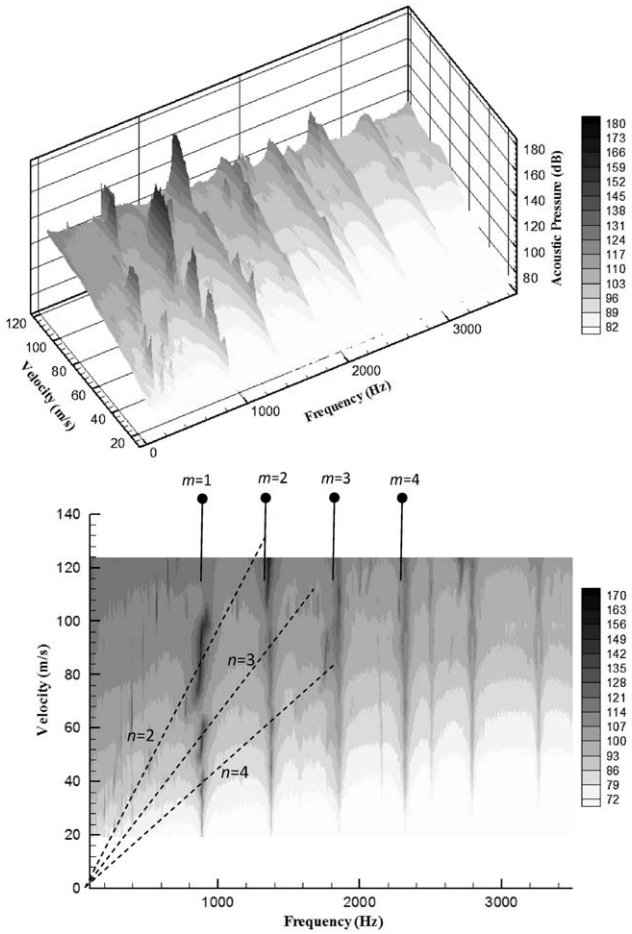

Fig. 26. Waterfall plot and 2-D pressure contours for $L/d = 3/2$, $d/D = 4/12$; m is the diametral mode number, n is the free shear-layer mode number.

At a certain flow velocity, more than one diameter mode can be susceptible to excitation by different free shear-layer modes. In this case, one of the diametral modes eclipses the other one(s) and dominates the aeroacoustic response. For example, in Fig. 14 ($L/d = 1$ and $d/D = 2/12$) between 60 and 70 m/s, the third diametral acoustic mode ($m = 3$) is not excited by the second free shear-layer mode ($n = 2$) because the first acoustic mode ($m = 1$) is excited strongly by the first shear-layer mode ($n = 1$). In this paper, this phenomenon is referred to as *mode selectivity*. Mode selectivity was found to be dependent on the cavity depth to pipe diameter ratio, d/D.

Figs. 31(a)–(c) show the dominant acoustic modes over the tested flow velocity range for three cavities of equal length ($L/D = 2/12$), but with different depths: $d/D = 1/12$, $2/12$ and $4/12$, respectively. Fig. 31(b) shows the same data from Fig. 13, but is included here to facilitate visual comparison. These figures illustrate the phenomenon of the susceptibility of different acoustic modes to excitation by various shear-layer modes. They also exemplify the dependence of this phenomenon on the cavity depth ratio. It is noteworthy that all three cavities have the same length, to ensure that the coincidence between the frequency of each shear-layer mode and a particular acoustic mode occurs at approximately the same flow velocity. For $d/D = 1/12$, the first diametral acoustic mode is not excited except over a very narrow velocity range near 70 m/s. In this case, the higher order acoustic modes seem to be more liable to excitation. On the other hand, for $d/D = 4/12$, the lower order acoustic modes are more liable to excitation. The cavity with $d/D = 2/12$ is an intermediate case where all modes are excited. This indicates that, for the deepest cavity ($d/D = 4/12$), the lower order acoustic modes are more susceptible to acoustic resonance than the higher order modes.

Recalling the results of the simulation of the acoustic modes, Fig. 11 shows that in the case of the deepest cavity ($d/D = 4/12$), the acoustic particle velocity amplitude at the cavity mouth decreases with the increase of the acoustic mode order. However, for the shallowest cavity ($d/D = 1/12$) the trend is reversed such that the particle velocity

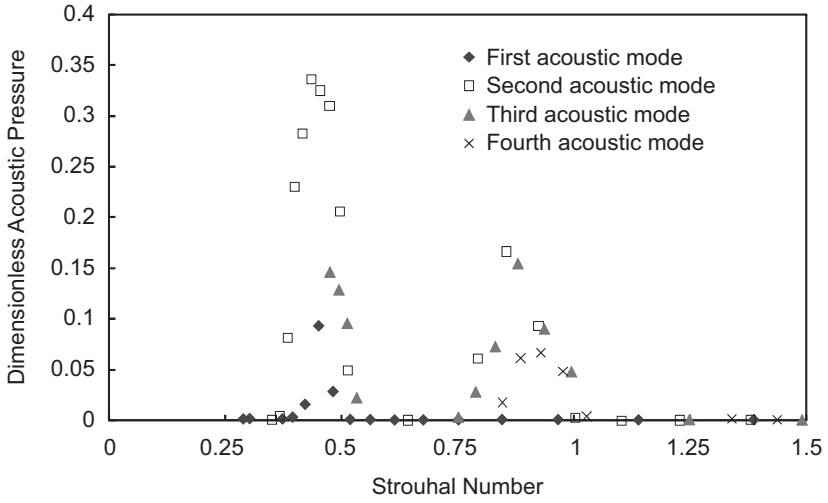

Fig. 27. Dimensionless pressure as a function of the Strouhal number for $L/d = 2$, $d/D = 1/12$.

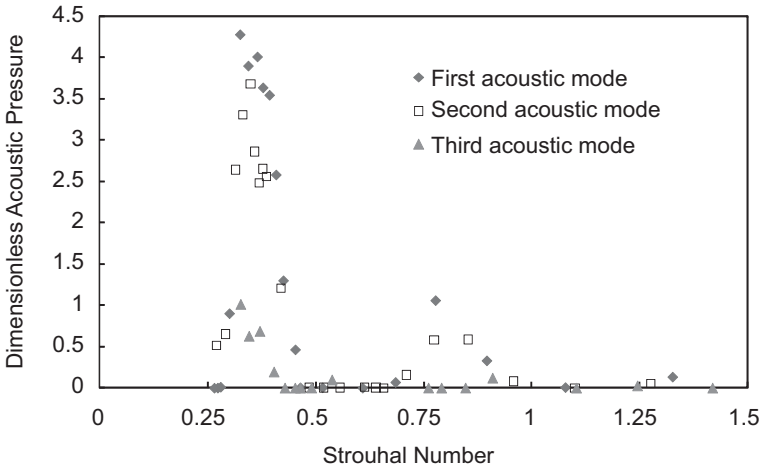

Fig. 28. Dimensionless pressure as a function of the Strouhal number for $L/d = 1/2$, $d/D = 4/12$.

increases with the increase of the acoustic mode order. It should be recalled here that more acoustic power is produced by the mode with the higher radial particle velocity. Thus, the effect of cavity depth on the acoustic particle velocity partially clarifies the phenomenon of mode selectivity of acoustic resonance and its dependence on the cavity depth. The results also provide new insight into the effect of changes in the diametral mode shapes on the aerodynamic excitation mechanism.

9. Conclusions

The characteristics of the self-excitation of acoustic diametral modes of an axisymmetric cavity–duct system were investigated experimentally. The acoustic response was measured for a range of flow Mach number up to 0.4. The results show that the axisymmetric cavity free shear layer can excite strongly the acoustic diametral modes. The excitation is self-sustainable for Mach numbers higher than 0.09. The pressure amplitude decreases with the increase of the cavity length to the pipe diameter ratio. The dimensionless amplitude drops by an order of magnitude when the cavity length to pipe diameter ratio increases from 1/6 to 1.

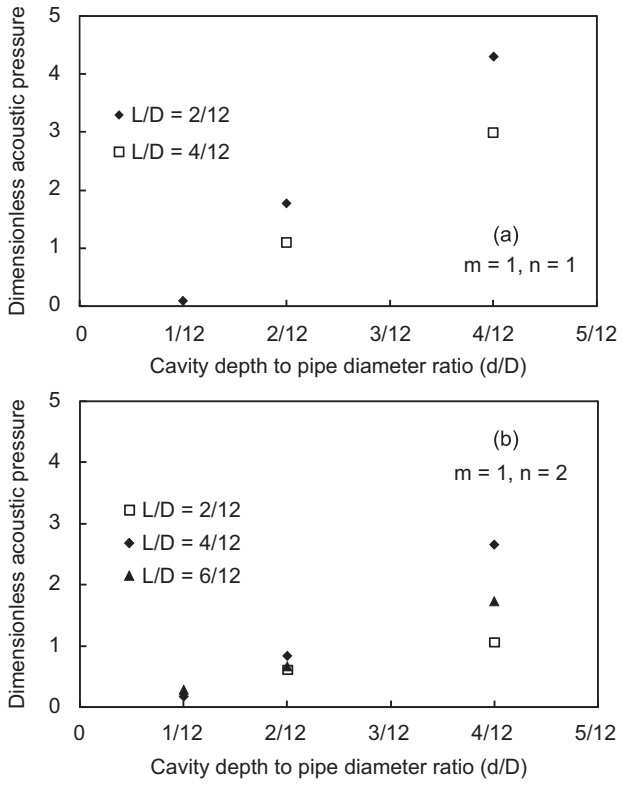

Fig. 29. Maximum dimensionless acoustic pressure of the first diametral mode for different cavity depths to pipe diameter ratios: (a) excitation by cavity first free shear-layer mode ($n = 1$) and (b) excitation by cavity second free shear-layer mode ($n = 2$).

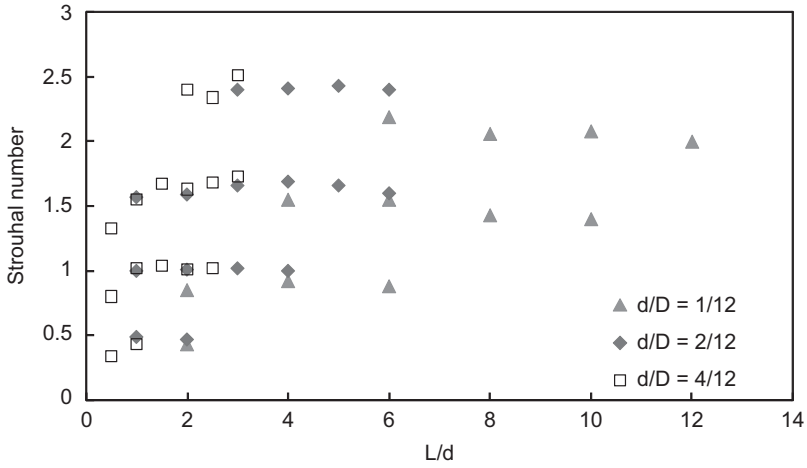

Fig. 30. Strouhal numbers of cavity free shear-layer modes for all tested cases.

The increase of the cavity depth results in a significant increase in the overall measured pressure amplitude. The trend of the change of the pressure amplitude with the cavity depth indicates that the resonance can be totally suppressed for cavities with $d/D = 5\%$ or smaller. The finite element analysis shows that, for a constant cavity length, the change in the cavity depth alters the amplitude of the acoustic particle velocity at the cavity mouth and consequently the contribution of the acoustic field to the acoustic power production in the way observed in the experiment. The amplitude of the

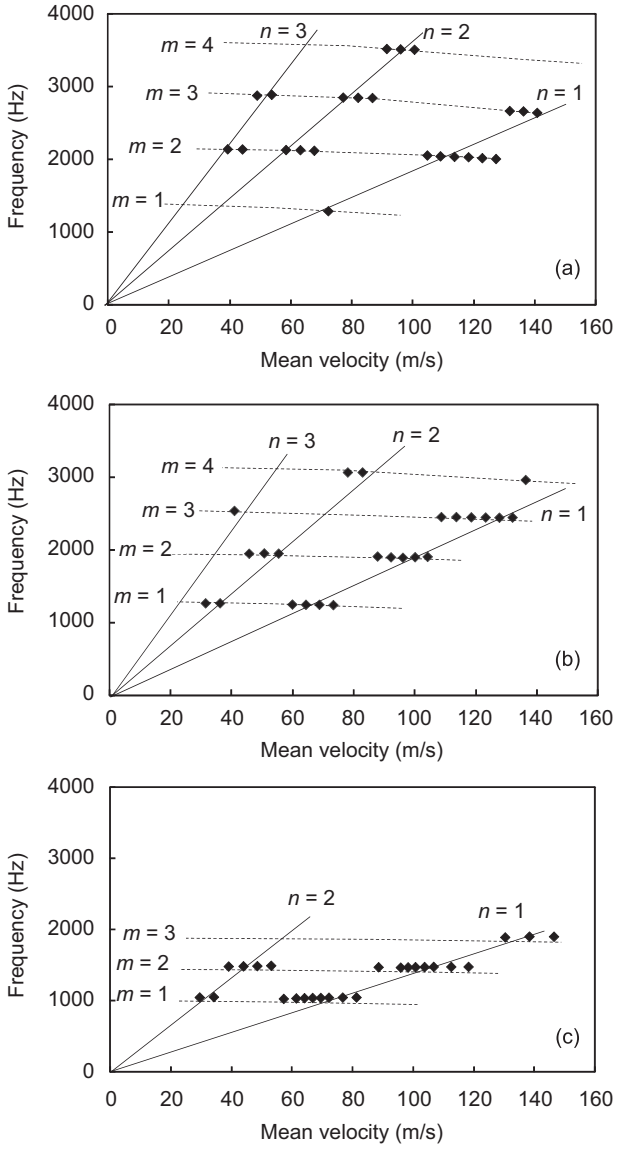

Fig. 31. Frequency of the dominant diametral acoustic modes: (a) $d/D = 1/12$, $L/D = 2/12$; (b) $d/D = 2/12$, $L/D = 2/12$; and (c) $d/D = 4/12$, $L/D = 2/12$ (m: the acoustic mode order, n: the free shear-layer mode number).

acoustic particle velocity depends also on the diametral mode order. Accordingly, the relative susceptibility to excitation of the different diametral modes depends on the cavity depth. For cavities with the largest depth ($d/D = 4/12$), the lower order diametral modes are more susceptible to excitation and dominate the acoustic response, while the higher order diametral modes dominate the acoustic response in the case of a small depth cavity ($d/D = 1/12$).

The longitudinal modes are excited for a relatively *long cavity* ($L/D > 1/2$). The amplitude of the longitudinal modes increases with the increase of both the cavity length and depth. In the cases of $d/D = 2/12$ and $4/12$, the excitation of the longitudinal modes dominates the system aeroacoustic response for cavity length to pipe diameter ratio larger than 5/6.

References

Ahuja, K.K., Mendoza, J., 1995. Effect of cavity dimensions, boundary layer and temperature on cavity noise on emphasis on benchmark data to validate computational aeroacoustic codes. NASA Contractor Report 4653

Ahuja, K., Chambers, F., 1987. Prediction and measurement of flows over cavities—a survey. AIAA-1987-166.
Bruggeman, J.C., Hirschberg, A., Van Dongen, M.E.H., Wijnands, A., 1991. Self-sustained aero-acoustic pulsations in gas transport systems: experimental study of the influence of closed side branches. Journal of Sound and Vibration 150, 371–394.
Davies, P., 1981. Flow-acoustic coupling in ducts. Journal of Sound and Vibration 77, 191–209.
Dequand, S., Hulshoff, S.J., Hirschberg, A., 2003. Selfsustained oscillations in a closed side branch system. Journal of Sound and Vibration 265, 359–386.
Flandro, G.A., 1986. Vortex driving mechanism in oscillatory rocket flows. Journal of Propulsion 2, 206–214.
Geveci, M., Oshkai, P., Rockwell, D., Lin, J.C., Pollack, M., 2003. Imaging of the self-excited oscillation of flow past a cavity during generation of a flow tone. Journal of Fluids and Structures 18, 665–694.
Hein, S., Koch, W., 2008. Acoustic resonances and trapped modes in pipes and tunnels. Journal of Fluid Mechanics 605, 401–428.
Hourigan, K., Welsh, M.C., Thompson, M.C., Stokes, A.N., 1990. Aerodynamic sources of acoustic resonance in a duct with baffles. Journal of Fluids and Structures 4, 345–370.
Howe, M.S., 1980. The dissipation of sound at an edge. Journal of Sound and Vibration 70, 407–411.
Keller, J.J., Escudier, M.P., 1983. Flow-excited resonances in covered cavities. Journal of Sound and Vibration 86, 199–226.
Kinsler, L.E., Frey, A.R., Coppens, A.B., Sanders, J.V., 2000. Fundamentals of Acoustics, Fourth edition. John Wiley & Sons, Inc, New York.
Koch, W., 1983. Resonant acoustic frequencies of flat plate cascade. Journal of Sound and Vibration 88, 233–242.
Kook, H., Mongeau, L., Brown, D.V., Zorea, S., 1997. Analysis of the interior pressure oscillations induced by flow over vehicle openings. Noise Control Engineering Journal 45, 223–234.
Krishnamurty, K., 1955. Acoustic radiation from two-dimensional rectangular cutouts in aerodynamic surfaces. NACA Technical Note No, 3487, USA.
Kriesels, P.C., Peters, M.C.A.M., Hirschberg, A., Wijnands, A.P.J., Iafrati, A., Riccardi, G., Piva, R., Bruggeman, J.C., 1995. High amplitude vortex induced pulsations in gas transport systems. Journal of Sound and Vibration 184, 343–368.
Lafon, P., Caillaud, S., Devos, J.P., Lambert, C., 2003. Aeroacoustical coupling in a ducted shallow cavity and fluid/structure effects on a steam line. Journal of Fluids and Structures 18, 695–713.
Nelson, P.A., Halliwell, N.A., Doak, P.E., 1983. Fluid dynamics of a flow excited resonance, Part II: flow acoustic interaction. Journal of Sound and Vibration 91, 375–402.
Nomoto, H., Culick, F.E.C., 1982. An experimental investigation of pure tone generation by vortex shedding in a duct. Journal of Sound and Vibration 84, 247–252.
Rockwell, D., Lin, J.C., Oshkai, P., Reiss, M., Pollack, M., 2003. Shallow cavity flow tone experiments: onset of locked-on states. Journal of Fluids and Structures 17, 381–414.
Rockwell, D., Naudascher, E., 1978. Review: self-sustaining oscillations of flow past cavities. ASME Journal of Fluids Engineering 100, 152–165.
Rockwell, D., Schachenmann, A., 1982. Self-generation of organized waves in an impinging turbulent jet at low mach numbers. Journal of Fluid Mechanics 117, 425–441.
Rossiter, J.E., 1962. The effect of cavities on the buffeting of aircraft. RAE Technical Memo, p. 754.
Schachenmann, A., Rockwell, D., 1980. Self-sustained oscillations of turbulent pipe flow terminated by an axisymmetric cavity. Journal of Sound and Vibration 73, 61–72.
Sarohia, V., 1977. Experimental investigation of oscillations in flows over shallow cavities. AIAA Journal 15, 984–991.
Smith, B.A., Luloff, B.V., 2000. The effect of seat geometry on gate valve noise. ASME Journal of Pressure Vessel Technology 122, 401–407.
Stoneman, S.A.T., Hourigan, K., Stokes, A.N., Welsh, M.E., 1988. Resonant sound caused by flow past two plates in tandem in a duct. Journal of Fluid Mechanics 192, 455–484.
Tam, C.R.W., Block, P.T.W., 1978. On the tones and pressure oscillations induced by flow over rectangular cavities. Journal of Fluid Mechanics 89, 373–399.
Tracy, M., Plentovich, E., 1993. Characterization of cavity flow fields using pressure data obtained in the Langley 0.3-meter transonic cryogenic tunnel. NASA Technical Memorandum 4436.
Ziada, S., Bühlmann, E.T., 1989. Flow impingement as an excitation source in control valves. Journal of Fluids and Structures 3, 529–549.
Ziada, S., Bühlmann, E.T., 1992. Flow-excited resonances of two side-branches in close proximity. Journal of Fluids and Structures 6, 583–601.
Ziada, S., Ng, H., Blake, C.E., 2003. Flow excited resonance of a confined shallow cavity in low Mach number flow and its control. Journal of Fluids and Structures 18, 79–92.
Ziada, S., Shine, S., 1999. Strouhal numbers of flow-excited acoustic resonance of closed side branches. Journal of Fluids and Structuers 13, 127–142.